Effect of Nitrate and Sulfate on Atmospheric Corrosion of 304L and 316L Stainless Steels

Cook, Angus; Padovani, Cristiano; Davenport, Alison

DOI:
10.1149/2.0921704jes

Document Version
Publisher's PDF, also known as Version of record

Citation for published version (Harvard):
Cook, AJMC, Padovani, C & Davenport, AJ 2017, 'Effect of Nitrate and Sulfate on Atmospheric Corrosion of 304L and 316L Stainless Steels', Electrochemical Society. Journal, vol. 164, no. 4, pp. C148-C163. https://doi.org/10.1149/2.0921704jes

Effect of Nitrate and Sulfate on Atmospheric Corrosion of 304L and 316L Stainless Steels

Angus J. M. C. Cook,[a] Cristiano Padovani,[b] and Alison J. Davenport[a,*,z]

[a]*School of Metallurgy and Materials, University of Birmingham, Edgbaston, Birmingham, West Midlands B15 2TT, United Kingdom*
[b]*Radioactive Waste Management Ltd., Curie Avenue, Harwell, Oxfordshire OX11 0RH, United Kingdom*

The effects of nitrate and sulfate salts on the chloride-induced atmospheric pitting corrosion of 304L and 316L stainless steel was investigated through automated deposition of droplets of magnesium and calcium salts. Nitrate was found to inhibit pitting under magnesium salt droplets when the ratio between the deposition density of nitrate anions and chloride anions was above a critical value, which was the same for both 304L and 316L. This critical ratio was found to decrease with increasing humidity. Sulfate was also observed to inhibit pitting for $MgCl_2 + MgSO_4$ mixtures, but only at higher humidities. Sulfate did not show any inhibition for $CaCl_2 + CaSO_4$ mixtures, an effect attributed to the low solubility of $CaSO_4$. At low relative humidities, precipitation of the inhibiting salt was observed, leading in some cases to crevice-like corrosion under salt crystals. The pitting behavior was explained in terms of the thermodynamic behavior of concentrated solutions.

 [DOI: 10.1149/2.0921704jes]

Manuscript submitted August 5, 2016; revised manuscript received February 1, 2017. Published February 9, 2017.

In the UK, stainless steel is used to package intermediate level radioactive waste, ILW, which is characterized by relatively large volumes and variable levels of radioactivity.[1] Whatever the strategic approach to its management[c], most ILW has been packaged in thin-walled containers (2.3–6 mm thick, typically grades 304L or 316L, UNS S304003 and UNS S316003, respectively) and will undergo long periods of exposure to atmospheric conditions, either in surface or underground facilities prior to permanent disposal.

During these periods, waste containers will be exposed to regimes of varying temperature and relative humidity (RH), as well as to chloride-containing salts arising from aerosol deposition. As a result, it is important to identify suitable storage conditions to ensure durability of waste containers, in particular to avoid conditions associated with the development of pitting and, even more importantly, atmospherically-induced stress corrosion cracking (AISCC).[2,3]

Monitoring of ILW storage facilities and other indoor locations considered broadly representative of ILW stores suggests that temperature and relative humidity, which are key parameters in the development of atmospheric corrosion, are expected to vary between ∼0–30°C and ∼30–100% RH, respectively.[3] Ionic chemical species deposited on surfaces after relatively long periods of indoor storage found in swab tests in a variety of real storage facilities include calcium, magnesium, sodium, potassium, chloride, nitrate and sulfate ions. Inside the storage buildings surveyed, chloride deposition densities were found to be below ∼20 μg/cm^2, with deposition rates of the order of 1 μg/cm^2 per year estimated.[3] With such a deposition rate, the chloride deposition density could increase to ∼100 μg/cm^2 over the next century.

In atmospheric conditions relevant to this work, a number of tests have been carried out to evaluate the atmospheric pitting corrosion of stainless steel in the presence of chloride deposits (e.g., Refs. 2, 4–6) but none of these have been carried out in the presence of ionic species other than chloride. In particular, anions such as nitrate and sulfate, which are likely to be present in amounts comparable to chlorides in waste stores,[3] have been shown to inhibit corrosion processes in bulk solutions above specific critical ratios to the chloride ion.[7–17]

The concentration of $MgCl_2$ in equilibrium with an ambient RH of 90% is ∼1.5 M, and increases with decreasing humidity.[18] Inhibition ratios found in bulk experiments (typically at concentrations below 1 M) may not be representative of atmospheric conditions.[19] For example, the relative humidity in typical stores is expected to vary between ∼30% and ∼100% RH (equivalent to $MgCl_2$ at saturation (∼5 M) and 'infinite dilution', respectively).[20] Furthermore, atmospheric corrosion differs from full immersion corrosion in a number of other ways. The thin electrolyte layer both allows easier oxygen access to the metal surface, and may limit ion migration and current flow through the electrolyte. Conversely, the increasing solution concentration decreases the solubility of O_2, which will decrease the access of oxygen to the metal surface. Furthermore, the area available for the cathodic reaction is limited by the coverage of the electrolyte (i.e. the footprint of the droplet).[20,21]

Methods employed to simulate atmospheric corrosion conditions used in previous studies include the formation of extended thin-films of electrolyte,[22–24] ink-jet printing of salt layers that deliquesced to form droplets,[21,25,26] and direct droplet deposition.[2,20,27–29] The current work uses automated deposition of combinatorial arrays of droplets to identify inhibiting nitrate:chloride deposition density ratios (NDD:CDD) and sulfate:chloride deposition density ratios (SDD:CDD) for both 304L and 316L stainless steels, at ∼31°C and several fixed exposure humidities.

The corrosion that develops in stores is likely to be a result of deliquescence of a salt layer that accumulates over time via aerosol deposition. However, in the current work, deposition of salt droplets was selected as a simple reproducible method for generating a wide range of different solution chemistries on a single metal plate. The findings from the current work are likely to be conservative, since initiation takes place under a relatively large droplet with a correspondingly large cathodic area compared with the smaller, patchy and disconnected areas of electrolyte that are likely to form in the early stages of aerosol deposition.

The aim of this study is to evaluate the inhibiting effects under low temperature atmospheric conditions, representative of storage environments for radioactive wastes as well as many other indoor facilities.[3] Beyond helping to build a comprehensive picture of the key factors controlling long-term atmospheric corrosion processes, this information is being used in the development of a corrosion prediction model.[30]

Experimental

Materials and surface preparation.—Type 304L and Type 316L stainless steel plate (UNS S30403 and UNS S316003, respectively) with 3 mm thickness was provided by Aperam France in a cold rolled and solution annealed (1040–1100°C, forced air cooling) condition.

*Electrochemical Society Member.
[z]E-mail: a.davenport@bham.ac.uk

[c]The strategy for the management of higher activity radioactive waste in England, Wales and Northern Ireland is currently permanent disposal in a geological disposal facility (GDF). After interim storage in surface facilities, radioactive wastes will be emplaced in a GDF which will then be backfilled and sealed. In Scotland, the current strategy for the management of higher activity radioactive wastes is long-term storage and near-surface disposal.[2]

Table I. Cast analysis provided by foundry for 304L and 316L stainless steel plate.

	Chemical Analysis (wt-%)											
Alloy	*C*	*Si*	*Mn*	*Ni*	*Cr*	*Mo*	*Ti*	*N*	*S*	*P*	*Co*	*Fe*
304L	0.023	0.44	1.46	8.00	18.08	–	–	0.072	0.0033	0.032	0.171	Bal.
316L	0.024	0.38	1.25	10.04	16.55	2.000	–	0.044	0.0032	0.034	0.189	Bal.

A cast analysis is provided in Table I. Plate was cut to appropriate size (either 30 × 50 or 25 × 75 mm) and mounted to aid handling. The samples were wet-ground to P800 grit using SiC discs such that the rolling direction of the alloy was perpendicular to the final grinding direction.

Samples were then ultrasonically cleaned in and then rinsed with >15 MΩ · cm de-ionized (DI) water (Millipore), dried under an air-stream, and left in a sheltered, ambient lab environment for 24 hours before deposition (20–26°C, 18–54% RH). It should be noted that the surface finish used in the current work is highly reproducible, but not identical to the surface finish of ILW containers, which are typically wet bead blasted.[31]

Solution arrays.—Stock solutions of $MgCl_2$, $CaCl_2$, $Mg(NO_3)_2$, $CaSO_4$ and $MgSO_4$ were made using ACS grade reagents: $MgCl_2 \cdot 6H_2O$, $CaCl_2 \cdot 2H_2O$, $Mg(NO_3)_2 \cdot 6H_2O$, $CaSO_4 \cdot 2H_2O$ (Sigma-Aldrich) and $MgSO_4 \cdot 7H_2O$ (Arcos Organics) and >15 MΩ · cm DI water (Millipore). Due to the low solubility of $CaSO_4$, a suspension was maintained using a magnetic stirrer during solution handling. Stock solutions were described in terms of anion concentration, and were approximately 1.0, 0.6 and 0.4 mol/L for chloride, nitrate and sulfate (apart from $CaSO_4$) solutions, respectively. The $CaSO_4$ stock solution was made to 0.26 mol/L.

Arrays of solutions with combinatorial ratios of anions were prepared from the stock solutions by a MultiPROBE II Ex automated liquid handler (Packard Biosciences) via serial dilution. Solutions were stored in well plates before deposition.

Two types of arrays were used:

- The first approach ('logarithmic' tests) varied both the chloride deposition density (CDD, mass per unit area of Cl^-, between 8.5–850 μg/cm^2) and either the nitrate or sulfate deposition densities (NDD, mass per unit area of NO_3^- or SDD, mass per unit area of SO_4^{2-}, between 0–850 μg/cm^2) 'logarithmically' across the same plate, with multiple plates used to replicate experiments (Figure 1a).
- The second ('linear' tests) consisted of a fixed CDD (~1200 μg/cm^2) across an entire plate, with linearly increasing NDD or SDD across the width of the plate. In these arrays, the NDD or SDD was varied linearly between 0 μg/cm^2 and an upper value chosen for each experiment (Figure 1b). It should be noted that the CDD chosen for these linear tests (~1200 μg/cm^2) is significantly higher than the range of CDDs expected in a store environment (up to ~100 μg/cm^2).[3] This was done in order to provide an aggressive environment, so that any inhibiting effects could be clearly identified.

For logarithmic arrays both 304L and 316L plates were investigated. For linear arrays only a single alloy was used for each exposure condition (salt type, humidity).

When evaluating inhibitor/chloride deposition densities (IDD:CDD) from the logarithmic and linear variation tests, it should be noted that the logarithmic variation tests provide better statistics (≥12 trials for IDD:CDD between 10–0.1) but larger increments (logarithmic IDD:CDD increments of 0.3, 1, 3 etc.), while the linear variation tests provide poorer statistics (4 trials per condition) but finer increments (linear NDD:CDD increments of ~0.17).

Additionally, pure $MgCl_2$ droplets (i.e. droplets with no inhibiting salt additions) were used as control tests to assess the aggressiveness of the exposure conditions and provide a baseline for comparison with the tests containing salt mixtures. These control droplets covered the same range of CDDs as tested in the mixed salt systems (i.e. 0.85–1200 μg/cm^2)

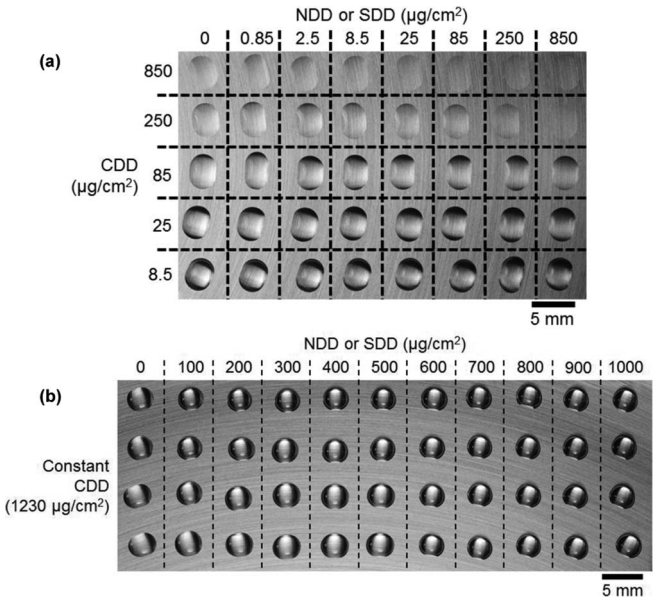

Figure 1. Array design for (a) logarithmic variation (3.3 mm diameter droplets) of both nitrate or sulfate deposition density (NDD or SDD) and chloride deposition density (CDD), (b) Linear variation (3.0 mm diameter droplets) of nitrate or sulfate deposition density (NDD or SDD) with chloride deposition density (CDD) kept constant. Images acquired after deposition, before exposure period. Note that values in linear variation in NDD or SDD on (b) are given as examples. Actual values are indicated with relevant experiments.

Droplet deposition and exposure.—Deposition of droplet arrays was automated using the MultiPROBE II Ex. Droplet volume at deposition was 4 μL unless otherwise stated, and droplets are referred to by their deposition volume in the text. On logarithmically-varying tests, freshly-deposited droplets had an area of 8.4 ± 0.3 mm^2. On linearly varying tests freshly-deposited droplets were measured to give an area of 7.1 ± 0.4 mm^2. It is thought that differences in deposited solution concentration are the result of different spreading behavior immediately after deposition, with the higher concentration solutions (used in the linear variation tests) showing lower spreading. Comparisons between photos taken after deposition, and photos taken after exposure showed no evidence of spreading during exposure. Droplets were typically elliptical, extending preferentially along the grinding lines with an average aspect ratio of ~1.2. The droplet diameters quoted below are the diameter of a circular droplet with the same mean droplet area. For 4 μL droplets with a mean area of 8.4 ± 0.3 mm^2, the equivalent diameter is ~3.3 mm. 4 μL droplets with an area of 7.1 ± 0.4 mm^2 give an equivalent diameter of ~3.0 mm.

Plates with linear NDD or SDD variation took ~10 minutes for deposition to finish, with no observed drying of the droplets in the ambient lab conditions. Plates with logarithmic CDD and NDD or SDD variation took ~40 minutes for deposition to finish. When ambient humidity was lower than the exposure humidity, these plates were suspended over a water bath during deposition to increase the local

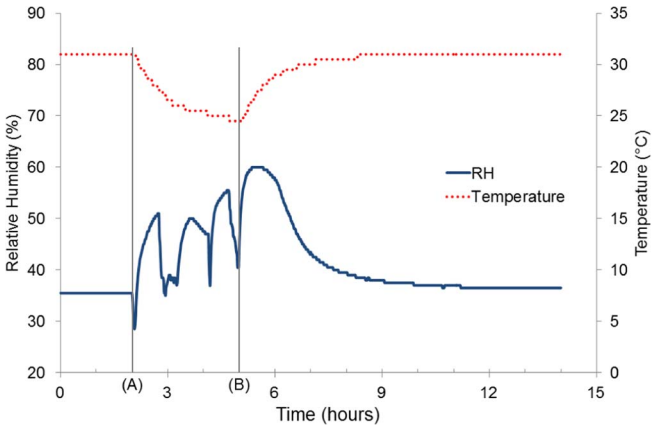

Figure 2. Data from temperature and humidity logger inside desiccator containing saturated $MgCl_2$ during sample placement plotted as a function of time from the beginning of droplet deposition onto the first batch of samples. The desiccator was taken out of the temperature chamber at (A). Between (A) and (B) 2nd–4th batch of samples underwent deposition and placement within the desiccator, with the deposition of the last (4th) batch of samples beginning ∼40 minutes preceding (B). The desiccator put back in oven at (B). Similar transient humidity increases were observed in all experiments just after sample insertion.

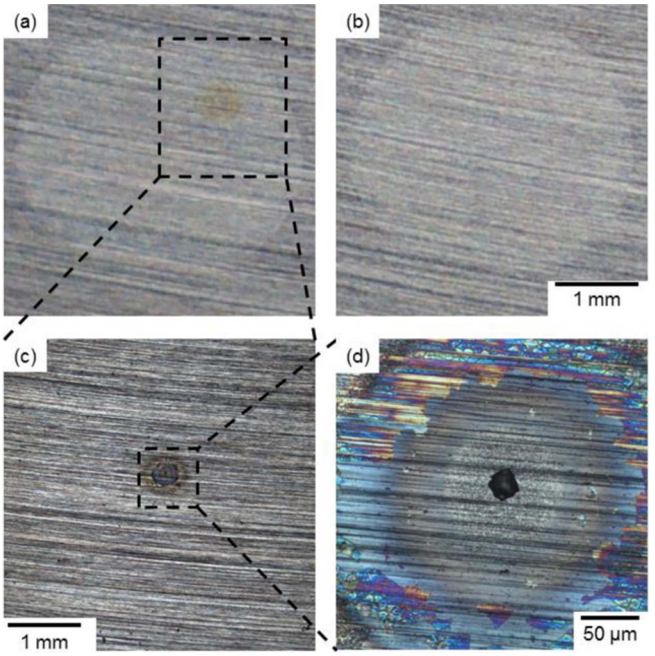

Figure 3. Example of the criterion for visual detection limit of pitting corrosion employed in the tests. (a) "pitted" droplet based on the observation of a rust stain (304L, 4 µL droplet, NDD:CDD of 2.5:8.5, 1 week exposure at 31°C, 46% RH), (b), "uncorroded droplet", no rust observed (304L, 4 µL droplet, NDD:CDD of 2.5:2.5, 1 week exposure at 31°C, 46% RH). (c) and (d), details of the pit from the droplet shown in (a), indicating that pits as small as 10s of µm in diameter were successfully detected by observation of the corrosion product from low magnification images.

humidity. Local humidity was typically increased by ∼5–10% RH by this method.

Where a test used a $CaSO_4$ suspension, an automated pipette was used to mix the suspension thoroughly, before aspirating sufficient solution for a single deposit. Each solution droplet was deposited individually, with the pipette tip returning to the stock solution well-plate each time to re-mix the solution. Due to the much longer deposition time required for this method (∼7 hours), $CaSO_4$ solutions were deposited first and allowed to dry before being over-deposited with a 2 µL droplet of the relevant chloride solution. Where the test with $CaSO_4$ employed a sulfate deposition density of 0 µg/cm^2, the area was pre-deposited with DI water. $CaSO_4$ coverage was generally fairly uniform, though in droplets with higher amounts of $CaSO_4$ the particles appeared to accumulate slightly toward the center of the droplet after being over deposited with $CaCl_2$, with deposits shrinking slightly back from the edge of the droplet.

Sample exposure.—After deposition, samples were photographed and placed within a selected exposure environment. Temperature was always set to 30°C. Humidity was controlled via saturated salt solutions within a desiccator ($MgCl_2$, K_2CO_3, NaBr or NaCl). The expected humidity fixed points (HFP) for the above salts at 30°C are 32.4 ± 0.2% RH, 43.2 ± 0.5% RH, 56.0 ± 0.4% RH and 75.1 ± 0.2% RH, respectively.[32] Samples were exposed alongside a temperature and humidity data logger (Lascar Electronics) to verify their exposure conditions. Samples were exposed for a period of 7 days, with previous preliminary work having shown that for CDDs between 10–1000 µg/cm^2 the majority of corrosion processes on 304L initiated within ∼48 hours of sample exposure.

Humidity verification.—The humidity within the desiccators was largely constant during the 7 day exposure. A significant divergence, common across all experiments, was observed just after samples were placed into the desiccator. At this time, the humidity was seen to increase sharply before slowly decreasing back to equilibrium (Figure 2). This was attributed to the evaporation of the dilute droplets as they equilibrated with the desiccator environment.

In previous work under pure magnesium chloride droplets on 304L, pits were observed to initiate within ∼1 hour of deposition, and so initiation under some droplets is expected to occur during this period of high humidity.[33] This was not expected to influence the results of the experiment, however, as the exposure conditions within the desiccator are thought become more aggressive over time as the system equilibrates (i.e. increase in temperature, increase in solution concentration), and it is assumed that any corrosion sites which initiated under higher humidity, lower temperature conditions would also have initiated under a constant higher temperature and lower humidity. In the general case, however, this humidity transient may affect systems where some of the samples contain dry salts at deposition, which may then deliquesce during the humidity transient, allowing corrosion to occur in this period. It may also affect the results of mixed binary chloride – inhibitor systems where the inhibitor becomes less effective at higher humidities (not expected in the current systems).

Average steady state temperature and humidity readings are given in Table II. In general, all samples to be exposed to a particular environmental condition were exposed together within the same desiccator. The exception to this was $MgCl_2$ + $Mg(NO_3)_2$ droplets on 304L samples at 46% RH, which were exposed separately to the rest. These data are highlighted in Table II.

Sample analysis.—Samples were photographed after exposure, washed in DI water, and photographed again. These photographs were used to assess whether or not corrosion had taken place under a given droplet. Corrosion sites were examined under an optical microscope.

Criteria used to interpret the tests.—A given droplet composition was deemed to allow/inhibit corrosion (pitting) based on the appearance of a rust stain. As examples, Figure 3a is considered a "corroded" droplet, while Figure 3b is considered a droplet where corrosion did not occur. The smallest pits detected from the observation of rust patches were ∼10–20 µm in diameter.

In some conditions (usually lower humidities), solid salt deposits precipitated out of solutions, and some droplets showed evidence of both precipitation and corrosion. Corrosion may be able to occur within a droplet with a nominally high inhibitor:chloride ratio if preceded by precipitation of the inhibitor, as precipitation within a

Table II. Nominal exposure conditions compared with measured exposure conditions. Recorded data given as average ± s.d., instrument error shown in header. Averages do not include humidity peak after sample insertion, common to every experiment (Figure 2).

Experiment	Temperature (°C)		Relative humidity (% RH)	
	Nominal	Recorded ± 0.5	HFP (Salt)	Recorded ± 3.0
$MgCl_2 + Mg(NO_3)_2/MgSO_4$ (Logarithmic)	30	31.2 ± 0.2	33 ($MgCl_2$)	35.5 ± 0.1
	30	31.5 ± 0.0*	43 (K_2CO_3)	46.0 ± 0.1*
	30	31.0 ± 0.2	43 (K_2CO_3)	46.8 ± 0.2
	30	31.4 ± 0.2	59 (NaBr)	58.3 ± 0.4
$MgCl_2 + Mg(NO_3)_2/MgSO_4$ (Linear)	30	31.0 ± 0.0	33 ($MgCl_2$)	34.7 ± 0.2
	30	31.0 ± 0.0	43 (K_2CO_3)	47.0 ± 0.1
	30	31.0 ± 0.1	59 (NaBr)	58.0 ± 0.2
$CaSO_4 + MgCl_2/CaCl_2$	30	31.0 ± 0.1	43 (K_2CO_3)	45.5 ± 0.1
	30	30.7 ± 0.2	59 (NaBr)	57.9 ± 0.2
	30	30.5 ± 0.1	75 (NaCl)	76.4 ± 0.6

*= 304L samples with $MgCl_2 + Mg(NO_3)_2$ droplets, which were exposed in a separate test.

droplet may remove the inhibiting anion from solution. As such, all judgements of inhibition ratios were taken from droplets without any precipitates.

In order to highlight scenarios where an inhibiting salt might precipitate from solution, and to more fully investigate the thermodynamic modelling of the binary salt system, it was of interest to record cases where precipitation had occurred due to environmental factors, i.e. when the exposure environment had led to precipitation within a droplet. It was important, however, to differentiate these cases from cases where precipitation may not have been caused purely by environmental factors, but by the presence of a corrosion site (though changing solution chemistry, or changes in surface morphology).[34]

When both corrosion and precipitation were observed under a droplet, the sequence of corrosion and/or precipitation was judged on the relationship between the corrosion products and the precipitate morphology. Figure 4 shows an example of the morphology of corrosion products and precipitates in these two cases. Figure 4a shows orange/brown corrosion products that are confined by precipitates, suggesting that in this case the corrosion product appeared after the precipitate (precipitation followed by corrosion). Conversely, in Figure 4b the corrosion product is found throughout the droplet and is independent of precipitate morphology, suggesting that it developed first, before the precipitation occurred. It should be noted that both types of behavior were observed for both nitrate- and sulfate-containing droplets.

In the following sections, cases of precipitation preceding corrosion are included in the text/graphs, indicating that the exposure environment was judged responsible. Cases where precipitation was thought to have followed corrosion have not been indicated, as in such cases it cannot be determined whether or not the precipitation was influenced by the changing solution chemistry or surface morphology brought about by corrosion.

Precipitates were identified visually from macrographs of the samples, so instances where only small levels of precipitation occurred may not have been recorded. Precipitates were not directly analyzed for composition, but in all cases were expected to be the inhibitor salt ($MgNO_3$ or $MgSO_4$), based on thermodynamic analysis.

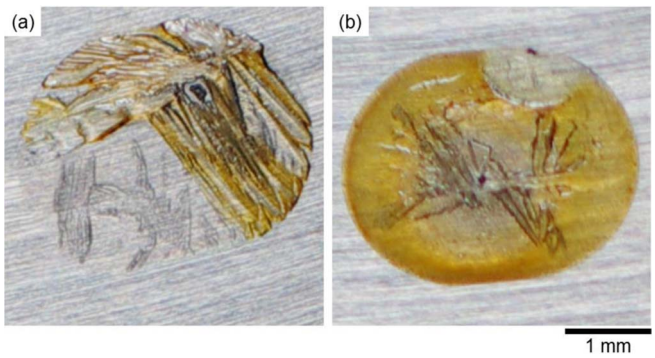

Figure 4. Examples of crystal growth (a) before and (b) after corrosion propagation under 3.3 mm diameter droplets on 304L at 31°C and 36% RH. (a) CDD 250 μg/cm^2, SDD 850 μg/cm^2. (b) CDD 850 μg/cm^2, NDD 250 μg/cm^2.

Thermodynamic analysis.—Thermodynamic analysis of the precipitation behavior of mixed salt solutions was carried out in order to complement the experimental work. Thermodynamic calculations were performed using OLI Stream Analyser Version 9.2, using the mixed solvent electrolyte model (MSE) main databank (H_3O^+ ion). All calculations were run at 30°C, 1 atm with vapor phases supressed.

Results

Control tests (no inhibitor present).—Table III shows the results of control tests carried out at different relative humidity values under pure $MgCl_2$ solutions on 304L and 316L. 316L samples had fewer occurrences of corrosion (rust patches) when compared with 304L. All corrosion was in the form of pitting. There appears to be a lower fraction of corroded droplets at intermediate RH (~45%), than at lower (~35%) or higher (~60%) RH.

In the case of 304L, the majority of control droplets (80–100% of tests) showed corrosion under the conditions tested, so any inhibition effect afforded by nitrate and sulfate salts should be very clear. However, in the case of tests on 316L, particularly at ~46% RH, far fewer droplets corroded than in the case of 304L (20–70% of tests). This indicates that the results on the potential inhibition effects of nitrate and sulfate need to be interpreted with care on 316L.

Table IV shows the results for a limited number of tests on smaller 2 μL (2.3 mm dia.) $CaCl_2$ and $MgCl_2$ droplets on 316L. These control tests were carried out to aid the interpretation of tests aimed at evaluating the inhibition properties of sulfate as $CaSO_4$ on 316L only, to complement the work with $MgSO_4$. Smaller droplets were used in order to fit a sufficiently large array onto each sample. In this limited set of tests no corrosion was seen under $MgCl_2$ droplets under the conditions tested. However, for $CaCl_2$, 2/5 droplets showed signs of corrosion, indicating that $CaCl_2$ is more corrosive than $MgCl_2$. While indicating a potentially higher corrosivity than $MgCl_2$, the limited incidence of corrosion in the control $CaCl_2$ tests (40% of tests) reinforces the idea that, particularly on 316L, the inhibition effects of sulfate need to be interpreted with care. Care should also be taken when comparing the $CaSO_4$ and $MgSO_4$ tests presented, as the different droplet volumes used are likely to have affected the likelihood of corrosion.[20]

Table III. Comparison between number of corroded 3.3 mm diameter $MgCl_2$ control droplets (as number and percentage) for 304L and 316L samples, exposed to humidities of 36% RH, 46/47% RH and 58% RH at 31°C. Results for all CDDs tested (8.5–850 μg/cm^2) are included.

	Number of corroded droplets (/40) and % corroded			
Relative Humidity (% RH)	304L		316L	
36	40	100%	27	68%
46,47	33	83%	9	23%
58	40	100%	19	48%

Table IV. Comparison between number of corroded 2 μL (2.3 mm diameter) $MgCl_2$ and $CaCl_2$ control droplets (as number and percentage) for 316L samples, exposed to humidities of 46% RH, 58% RH and 76% RH at 31°C. A 2 μL droplet of DI water was pre-deposited in the same location and allowed to dry before deposition of the salt solution. All tests had the same CDD of 1200 μg/cm^2.

	Corroded droplets (/5)			
Relative Humidity (% RH)	$CaCl_2$		$MgCl_2$	
46	2	40%	0	0%
58	0	0%	0	0%
76	0	0%	0	0%

Effect of magnesium nitrate on corrosion under magnesium chloride droplets.—Figure 5a shows an example of a test on 304L at 36% RH in which both chloride deposition density (CDD) and nitrate deposition density (NDD) are varied between 8.5 and 850 μg/cm^2 and 0 and 850 μg/cm^2, respectively. The micrographs show that at high CDD and low NDD, corrosion is observed in the form of pits surrounded by rust-like corrosion product. At high enough NDD, however, no rust is observed and corrosion is inhibited. Corrosion product coverage, which reflects the extent of pitting, varied with CDD, with higher CDDs leading to more extensive rust coverage and sufficiently low CCD (≤25 μg/cm^2) resulting in substantially less rust. Increasing the NDD for fixed CDD did not appear to affect the corrosion product coverage, until a cutoff where corrosion was inhibited, hence no rust was observed.

In all cases, corrosion was observed in the form of pits (Figures 5b and 5e). There was usually a single pit beneath each corroded droplet, although multiple pits were also observed under some conditions. Multiple pits were more common under lower CDD droplets (≤25 μg/cm^2) at 36% RH and 58% RH on 304L samples, but were also observed in other conditions. In some cases precipitation of salt crystals was observed. Under some precipitates (e.g. Figures 5d and 5g), pitting was observed.

Figure 6 shows the full set of results for both 304 and 316L under a range of humidities (36–58% RH). For 304L, at higher CDD and lower NDD values, all four tests for each condition showed corrosion (complete black circle) for most conditions. Above a critical NDD value, no corrosion was observed (open circle). However, for 304L at 36% RH (Figure 6a), as the NDD value increased further, some salt precipitation was observed in the droplets (superimposed light gray square). The precipitate was expected to be $MgNO_3$, as all tested humidities were above the deliquescence point for $MgCl_2$. At the highest NDD value (850 μg/cm^2), one or two examples of pits that were assumed to have initiated under salt crystals were observed (partially filled circle on a light gray square). This interpretation was based on the distribution of corrosion products (see Experimental Method).

In all conditions, 316L and 304L showed similar overall trends in corrosion susceptibility as a function of CDD and NDD, but 316L generally showed a lower probability of corrosion than 304L, particularly at 47% RH. In this paper, given the overall low corrosion probability for 316L (giving poorer statistics) and given that the effect of inhibition is more difficult to distinguish from the inherent corrosion resistance of the alloy (as shown by the control tests), inhibition ratios are generally evaluated on the basis of results on 304L and consistency with 316L is noted.

All tests indicated that corrosion inhibition is achieved on both alloys above specific NDD:CDD ratios. The effectiveness of nitrate as an inhibitor appears to be greater at higher humidity (i.e. less nitrate relative to chloride is required for inhibition at 58% RH than at 36% RH). No difference was observed between the critical ratio for corrosion inhibition for 304L and 316L. At low humidity (~36% RH), an inhibition ratio (NDD:CDD) between 1 and 3 on a mass basis can be inferred from these measurements (as shown in Figure 6 for 304L), decreasing to values below 1 at higher humidities (58% RH).

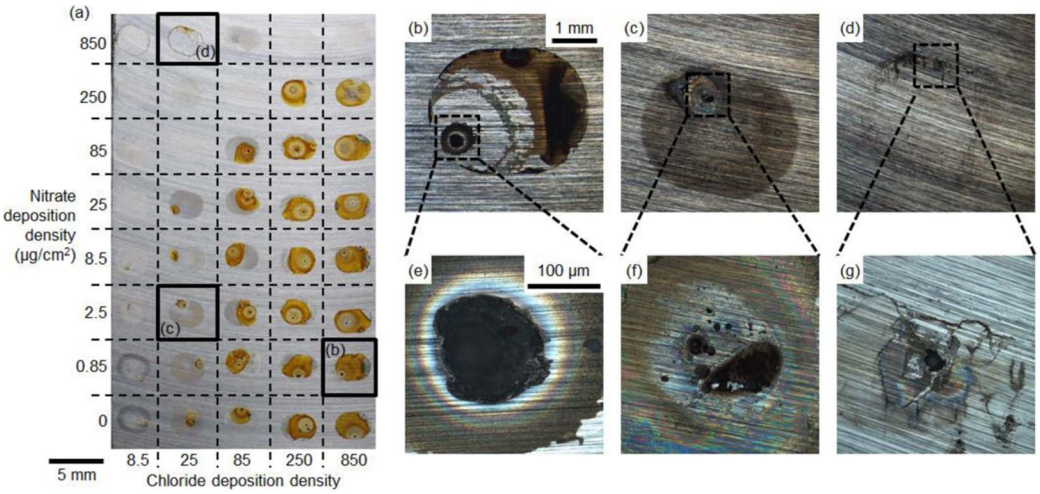

Figure 5. 304L plate with 3.3 mm diameter droplets of $MgCl_2 + Mg(NO_3)_2$ after 7 day exposure at 31°C, humidity of 36% RH, before DI rinse. (a) macrograph of the whole sample. (b-g) optical micrographs of droplets shown in (a) after DI rinse; (d,g) after further ultrasonic wash.

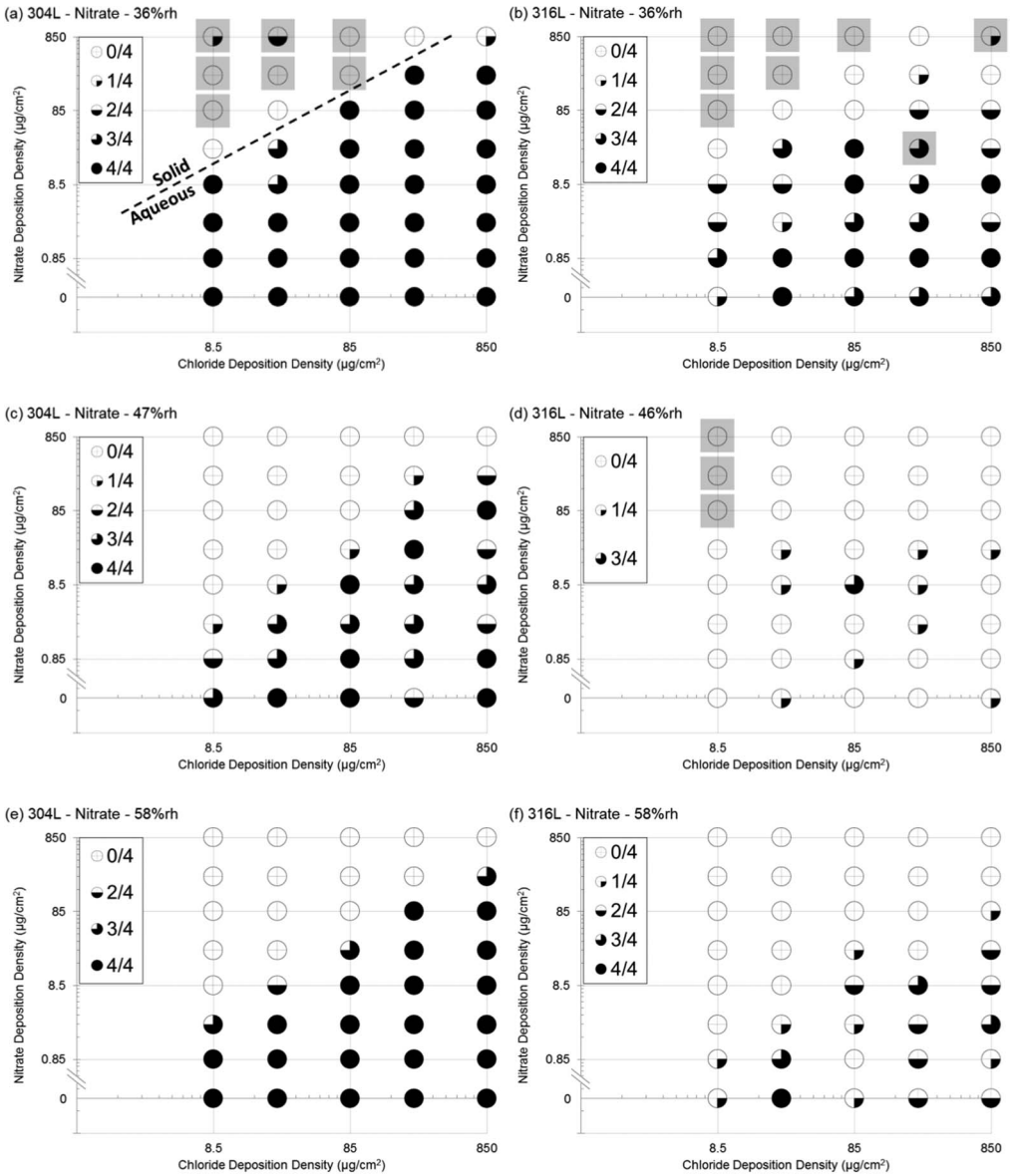

Figure 6. Data from 304L ([a], [c] and [e]) and 316L ([b], [d] and [f]) plates with 3.3 mm diameter droplets of $MgCl_2 + Mg(NO_3)_2$ solutions, exposed to humidity of 36% RH (a, b), 47% RH (c), 46% RH (d) and 58% RH (e, f). The fraction of each circle that is filled corresponds to fraction of droplets which showed corrosion (out of four tests). The data below the break in the y-axis indicates solutions with NDD of 0 $\mu g/cm^2$. Solution compositions where any salt crystals were observed that are assumed to have formed before any pitting (see Experimental Method) are indicated with gray squares. Salt crystal formation was highlighted if only a single instance within the four tests was observed. The thermodynamically predicted boundary for precipitation has been indicated in (a) calculated using OLI Analyser 9.2.,[18] NB: this boundary has not been indicated nor calculated on any other plot.

As noted above, at low humidities instances of corrosion sites developed after crystallization were observed (e.g. Figure 5a). These results indicate that, at low RH, inhibition may be lost or reduced due to the removal of nitrate from solution owing to formation of nitrate crystals and/or owing the formation of micro-crevices under these precipitates.

Further linear tests were conducted on 304L plate to explore conditions around the NDD:CDD threshold. In these tests the NDD was varied linearly, while the CDD was kept constant (at a value of ~1230 $\mu g/cm^2$). A typical example (plate exposed at 47% RH) is shown in Figure 7, while data from the full set of tests is shown in Figure 8.

As in the logarithmic tests, increasing the NDD showed clear evidence of corrosion inhibition. Similarly, increasing exposure RH reduced the NDD:CDD ratio required at which corrosion inhibition was observed (Figure 8). From these tests, with finer increments than the logarithmic tests, inhibition effects can be seen to commence for

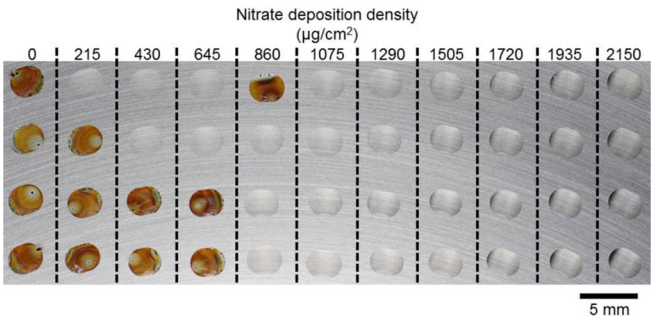

Figure 7. 304L plate with 3.0 mm diameter droplets of $MgCl_2 + Mg(NO_3)_2$, exposed at 31°C and at 47% RH for 7 days. Image taken after exposure, before DI rinse. Constant chloride deposition density of 1230 $\mu g/cm^2$ for each droplet, nitrate deposition density varied as shown.

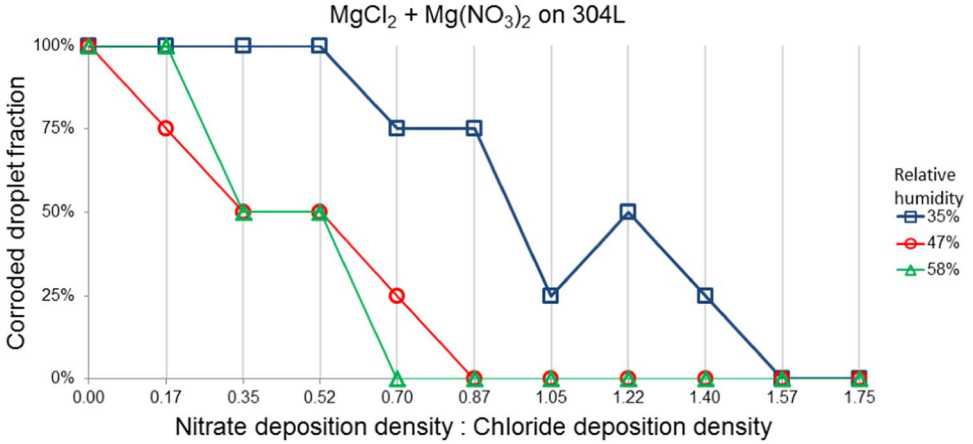

Figure 8. 304L samples with fixed CDD of at 1230 μg/cm^2 and linearly increasing nitrate deposition density (NDD) in steps of 215 μg/cm^2. 3.0 mm diameter droplets, exposed for 7 days at 31°C and humidity as shown. Plot shows number of corroded droplets (out of four repeats) for each NDD:CDD ratio and humidity.

NDD:CDD ratios above 0.1–0.5 on a mass basis, with full inhibition achieved at values of the order of 0.7–1.6, depending on exposure humidity.

Figure 9 shows the relationship between the critical inhibition nitrate:chloride ratio on both a deposited mass density basis (NDD:CDD) and a molar basis (NO_3^-:Cl^-), as a function of RH from both logarithmic variation and linear tests. For the logarithmic tests the "corrosion" point is the highest NDD:CDD ratio at which any corrosion was observed across all CDDs (0.85–850 μg/cm^2), excluding droplets with salt precipitates. The "no corrosion" point is the lowest value of the NDD:CDD ratio above the "corrosion" point (across all CDDs) at which no corrosion is observed. The linear variation data is plotted in the same way, but is relevant only for a single CDD (1230 μg/cm^2).

Figure 10 shows the inhibition ratios presented in Figure 6 as a function of chloride deposition density (for constant RH). In general, although there was variation in inhibition ratios with CDD, there was no clear trend in the variation, indicating no obvious dependence of the inhibition ratios on the deposition density.

Effect of magnesium sulfate on corrosion under magnesium chloride droplets.—Figure 11a shows an example (at a humidity of 46% RH) of a test varying both chloride deposition density (CDD) and sulfate deposition density (SDD) between 8.5–850 μg/cm^2 and 0–850 μg/cm^2 respectively on 304L. The micrographs show that corrosion is observed in most conditions, in the form of pits surrounded by rust-like corrosion product. In this example, corrosion was not prevented by the addition of sulfate for all tested values of SDD:CDD. As in the case of nitrate tests, corrosion (amount of rust observed) decreased significantly at low CDD, particularly below 25 μg/cm^2.

Corrosion was generally observed in the form of pits (Figures 11b and 11e), with multiple pits more common under low CDD droplets (≤25 μg/cm^2) at 36% RH and 58% RH humidity. Crevice-like attack was also observed under some droplets where $MgSO_4$ salt precipitates had acted as crevice formers (Figures 12c, 12d). Droplets with a high SDD:CDD ratio showed evidence of salt precipitation (Figures 11d and 11g). In general, the extent of precipitation was much greater than that observed in $MgCl_2$ + $Mg(NO_3)_2$ experiments, with precipitates observed at higher relative humidity and lower IDD:CDD ratios than those seen with $Mg(NO_3)_2$.

Figure 13 shows the full set of results for the effect of sulfate on both 304L and 316L at a range of relative humidities (36–58%). Salt precipitation was observed on both alloys across all humidities tested, particularly at higher SDD:CDD ratios. This was expected to be a $MgSO_4$ precipitate as all tested humidities are above the deliquescence point for $MgCl_2$. On 304L, no significant inhibition was observed at any relative humidity values across the full CDD range, though no corrosion was observed in high CDD (250 and 850 μg/cm^2) droplets with SDD:CDD ratios of 1 at 58% RH.

As noted above, from control tests (Table III) the probability of corrosion under magnesium chloride solutions on 316L (20–70%) is generally lower than 304L (80–100%), making it more difficult to

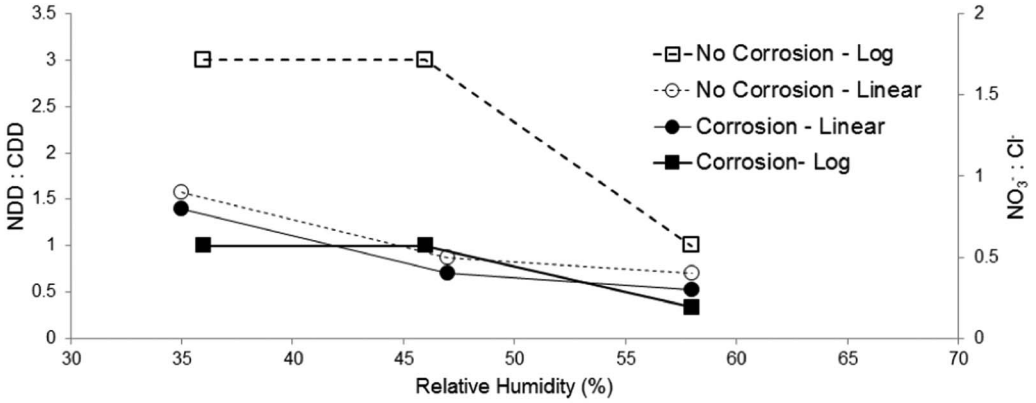

Figure 9. Nitrate:chloride inhibition ratio based on deposited mass (NDD:CDD) and molar basis (NO_3^-:Cl^-) as a function of RH. Data are taken from both logarithmic variation tests on 304L and 316L (Figure 6), and linear variation tests on 304L (Figure 8). Filled data points ("Corrosion") show the highest nitrate:chloride ratio at which pitting was observed across the range of CDDs examined. The open data points are the lowest value of the NDD:CDD ratio above the Corrosion point which showed no corrosion.

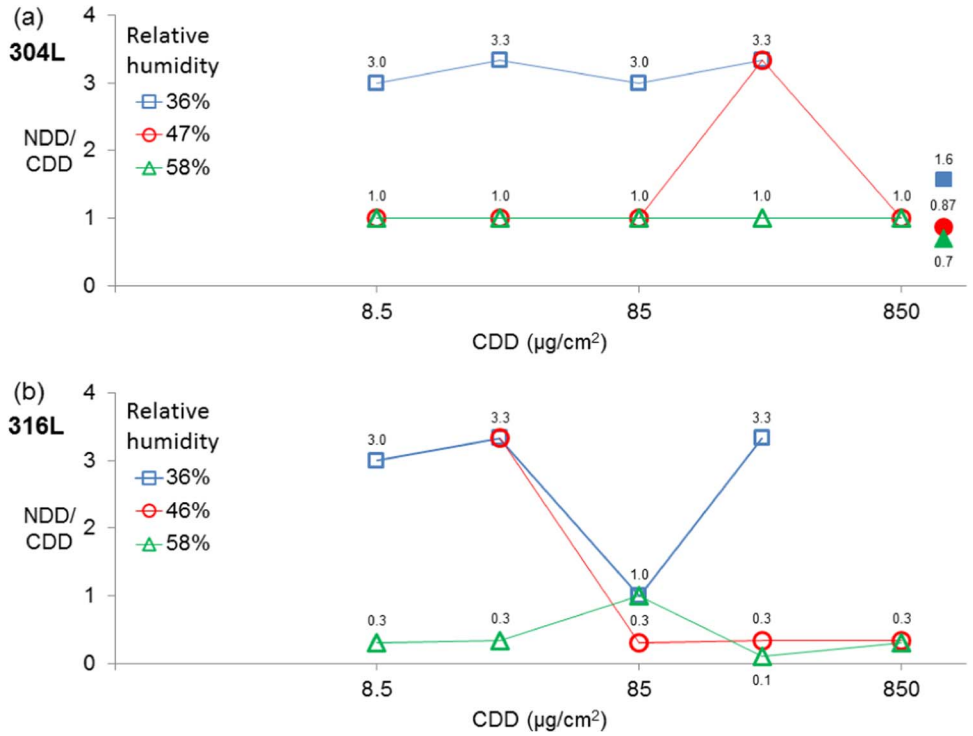

Figure 10. Nitrate:chloride inhibition ratios (NDD:CDD) on (a) 304L and (b) 316L alloys, at 36% RH, 46/47% RH and 58% RH, based on 'logarithmic tests' (Figure 6). Data points correspond to lowest NDD:CDD ratio where corrosion was not observed, data labels indicate NDD/CDD value. Droplets showing salt crystallization have been omitted. Filled data points in (a) at 1230 µg/cm^2 indicate ratios from linear tests (Figure 8). CDDs with no data point indicate conditions where inhibition was not observed.

assess inhibition effects on this alloy. However, comparing the probability of corrosion in Figure 13 with the results of Table III suggests that, whilst limited inhibition was observed at 36% RH, some inhibition was observed at a relative humidity of 58%, although the fraction of droplets showing corrosion was variable even at low SDD:CDD ratios. At 46% RH, the limited incidence and high variability of occurrence of corrosion in both the control and main tests was too great to determine any inhibiting effects. Corrosion variability was lower at 36% RH, but no clear trends in inhibitive effects of sulfate could be seen in this condition.

Further tests were conducted on 304L plate investigating linear variation in SDD while keeping CDD constant. The sample exposed to 58% RH humidity is shown in in Figure 14, while a summary of the whole set of tests at different humidity values is shown in Figure 15. Plates exposed at 35% RH and 47% RH showed no clear signs of inhibition with increasing SDD:CDD ratios. At 58% RH, however,

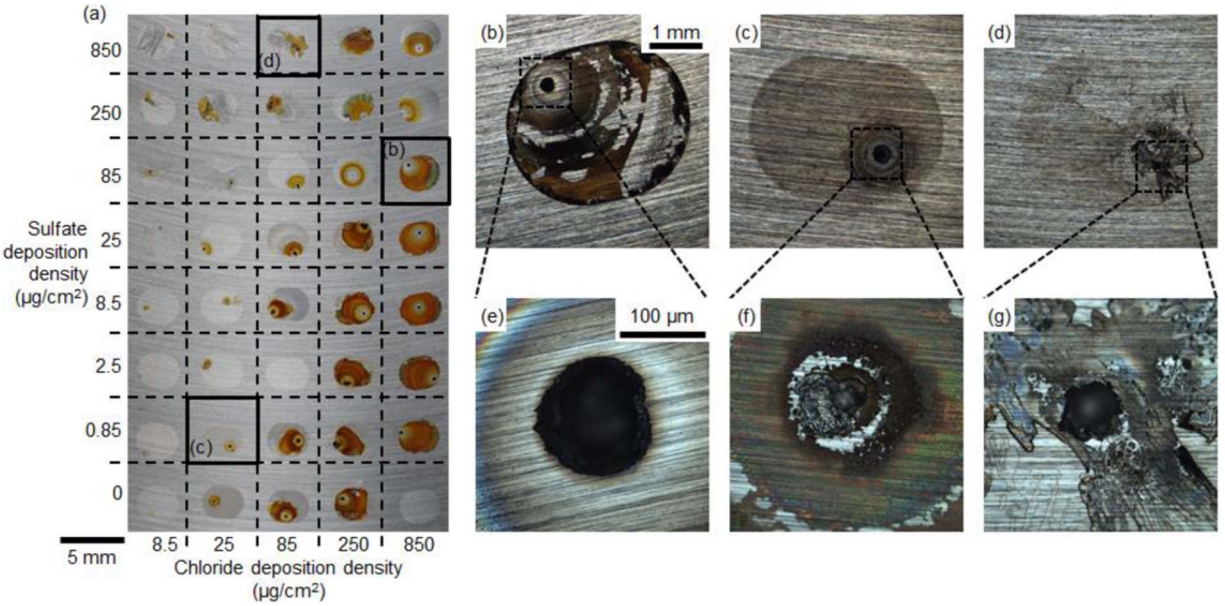

Figure 11. 304L plate with 3.3 mm diameter droplets of $MgCl_2 + MgSO_4$ after 7 day exposure at 31°C, humidity of 46% RH, before DI rinse. (a) micrograph of the whole sample. (b-g) optical micrograph of droplets shown in (a) after DI rinse; (d,g) after further ultrasonic cleaning.

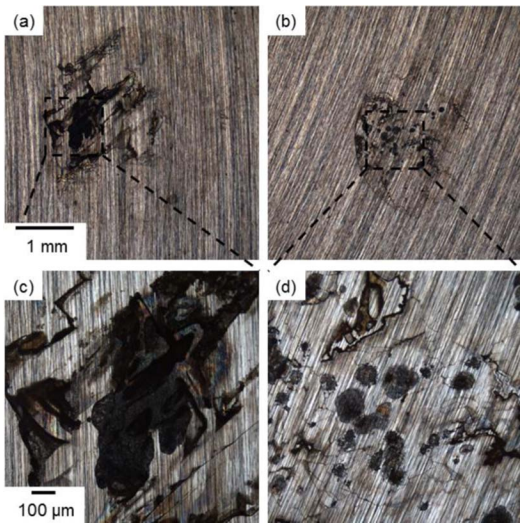

Figure 12. Examples of corrosion morphologies observed in 3.3 mm droplets of $MgCl_2 + MgSO_4$, where $MgSO_4$ precipitates affected corrosion site development. Both samples were 304L, exposed at 31°C. (a,c) 36% RH, 85 µg/cm^2 CDD, 850 µg/cm^2 SDD. (b,d) 58% RH, 8.5 µg/cm^2 CDD, 850 µg/cm^2 SDD.

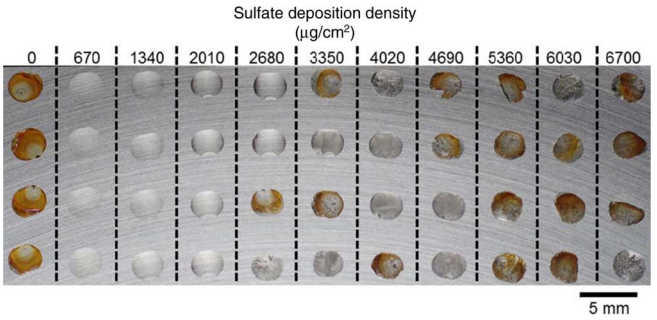

Figure 14. 304L plate with 3.3 mm diameter droplets of $MgCl_2 + MgSO_4$, exposed at 31°C and at 58% RH for 7 days. Image taken after exposure, before DI rinse. Constant chloride deposition density of 1230 µg/cm^2 for each droplet, sulfate deposition density varied as shown.

inhibition was observed between SDD:CDD ratios of 0.54 and 1.63. In droplets at higher SDD:CDD ratios, both salt precipitation and corrosion were observed, with all cases of corrosion occurring under precipitated droplets.

Effect of calcium sulfate on corrosion under magnesium chloride or calcium chloride droplets.—A preliminary investigation into the

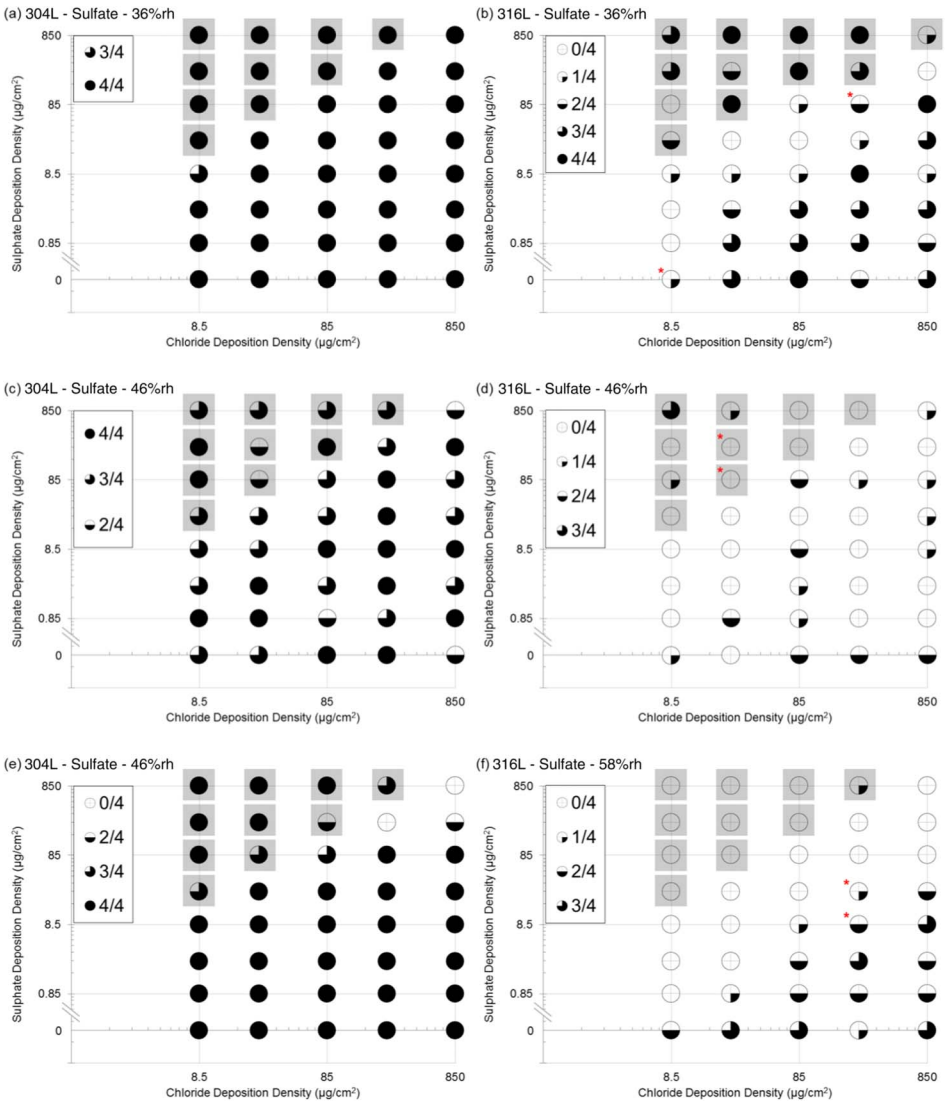

Figure 13. Data from 304L ([a], [c] and [e]) and 316L ([b], [d] and [f]) plates with 3.3 mm diameter droplets of $MgCl_2 + MgSO_4$ solutions, exposed to humidity of 36% RH (a, b), 46% RH (c, d) and 58% RH (e, f). The fraction of each circle that is filled corresponds to fraction of droplets which showed corrosion (out of four tests). The data below the break in the y-axis indicates solutions with NDD of 0 µg/cm^2. Solution compositions where any salt crystals were observed that are assumed to have formed before any pitting (see Experimental Method) are indicated with gray squares. Salt crystal formation was highlighted if only a single instance within the four tests was observed. Data points consisting of only 3 repeats have been indicated with an asterisk (*).

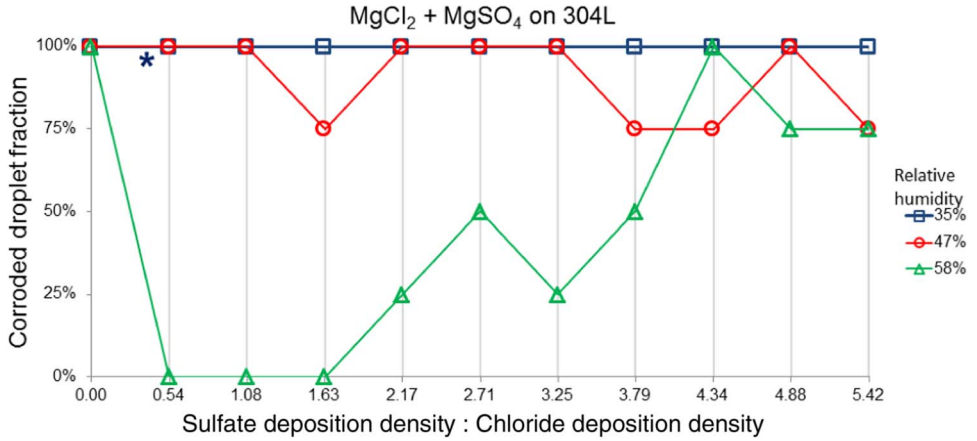

Figure 15. 304L samples with fixed CDD of at 1230 μg/cm^2 and linearly increasing sulfate deposition density (SDD) in steps of 670 μg/cm^2. 3.0 mm diameter droplets, exposed for 7 days at 31°C and humidity as shown. Plot shows number of corroded droplets (out of four repeats) for each SDD:CDD ratio and humidity. At an SDD:CDD ratio of 0.54 on the 35% RH test, two droplets were discounted due to a deposition error, and the pitting fraction is thus out of two (indicated by an asterisk *).

effects of calcium sulfate on corrosion was conducted under both magnesium and calcium chloride solutions. In contrast to the work presented so far, these tests were only carried out on 316L and across an elevated range of humidities (46–76% RH, compared to 36–58% RH used previously).

Figure 16 shows a typical sample used to investigate the effect of $CaSO_4$ on pitting under $CaCl_2$ solution on 316L stainless steel. 2 μL droplets were used (2.3 mm diameter). The CDD was kept constant at 1200 μg/cm^2, while the SDD was varied linearly between 0 and 1200 μg/cm^2. The $CaSO_4$ was pre-deposited onto the samples as a 2 μL suspended solution over a period of ~7 hours, and allowed to dry. The $CaSO_4$ was then over-deposited with chloride salt. Where an SDD of 0 μg/cm^2 was intended, the plate was pre-deposited with DI water.

No inhibition due to the presence of $CaSO_4$ was seen in these tests. In general the extent of corrosion was very low, with only 23/330 droplets showing signs of corrosion (16 of these corroded droplets can be seen in Figure 16). Similar to what observed in control experiments, corrosion occurred more frequently under $CaCl_2$ droplets than under $MgCl_2$ droplets (16/165 vs. 7/165 cases, respectively). The incidence of corrosion (about 10%), however, was similar to or even lower than that of the control experiments (20%), indicating limited (if any) inhibition effects. In all cases, corrosion was observed in the form of pits. $CaSO_4$ was highly insoluble, with a solid phase observed in all droplets with any $CaSO_4$ addition.

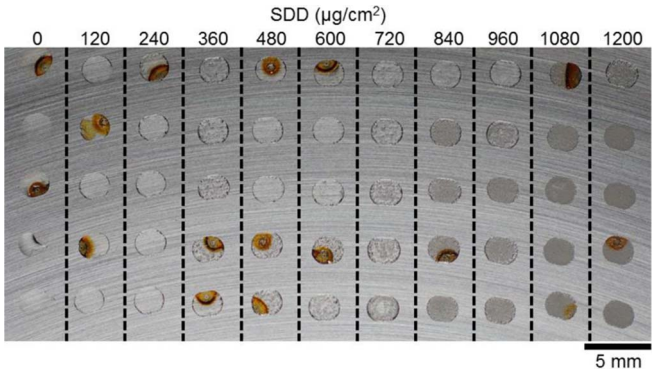

Figure 16. 316L with 2 μL droplets (2.3 mm diameter) with mixtures of $CaCl_2$ and $CaSO_4$. The CDD was 1200 μg/cm^2 for each droplet, while the sulfate deposition density (SDD) was as shown (pre-deposited as $CaSO_4$). 7 day exposure at 31°C, 46% RH. Image taken after exposure, before DI wash.

Discussion

The tests presented in this study were designed to evaluate the corrosion behavior of stainless steel in conditions of defined salt deposition densities. It was generally observed that, in both nitrate and sulfate tests, the corrosion product (rust) coverage under droplets (a good indicator of the amount of corrosion damage) was dependent on the CDD, with higher CDDs resulting in more extensive rust deposits (Figure 3a). Rust coverage tended to be relatively small at CCDs below 25 μg/cm^2 and greater at higher values. These observations are consistent with findings in pure $MgCl_2$ reported in previous studies.[2]

The expected range of CDDs within stores over the storage period is likely to be on the order of between 1–100 μg/cm^2, with the higher levels of CDD expected to accumulate toward the end of the storage period.[3] This range is lower than that in many of the results shown here. However, as shown in Figure 10 there is relatively little change in inhibition ratio with CDD, and there is generally good agreement between logarithmic and linear variation tests, which support the idea that inhibition ratios obtained at higher CDD ranges (as in this work) are likely to be applicable also to the lower CDD conditions found in stores.

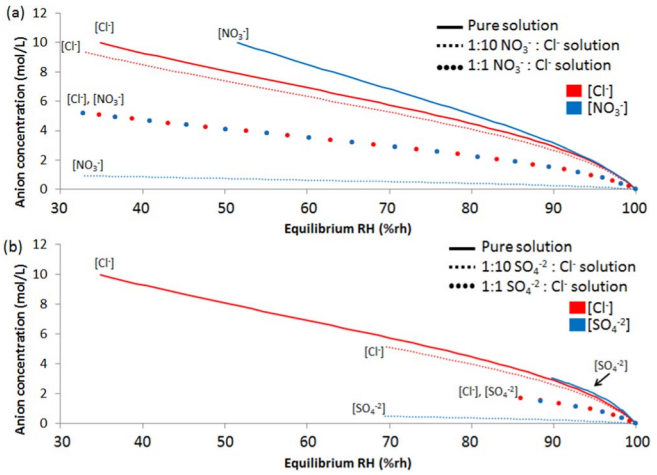

Figure 17. Calculated anion concentrations with respect to equilibrium RH, for solutions containing (a) $MgCl_2$ and $Mg(NO_3)_2$, including pure solutions; and (b) $MgCl_2$ and $MgSO_4$, including pure solutions.[18] Solution compositions are indicated on the relevant graphs. Note that the plots for solutions with a 1:1 anion composition overlay each other.

Exposure humidity.—The effect of the exposure humidity on the overall corrosion behavior in these tests can be evaluated by examining the control droplets (i.e. droplets with no nitrate or sulfate additions) on each sample. Across all logarithmic, tests the likelihood of corrosion occurring on both 304L and 316L was highest at a humidity of 36% RH (67 corroded droplets out of a total of 80), next at 58% RH (59/80), and lowest at 46% RH (42/80) (Table III). At lower humidity, the concentration of chloride in the droplet will be highest, providing a more aggressive chemistry for pit initiation (see Figure 17 for trends on anion concentration with respect to exposure RH).[4] According to this view, the most aggressive condition is expected to be at humidity just above the deliquescence point of $MgCl_2$, ~32% RH, with the solution decreasing in aggressiveness with increasing humidity.[32] A higher RH, however, will also increase the volume of the droplet, which, given that the droplets generally have the same diameter, leads to an increase in droplet height. In addition, in concentrated solutions, there is an increase in electrical conductivity as $MgCl_2$ solutions become more dilute.[33] Thus the IR-drop between any initiating anodic site and the cathode area is likely to be decreased as the RH increases, leading to a larger interfacial potential to drive the corrosion reaction.[21,33] It is speculated that the lowest level of observed pitting at 46% RH (particularly in control tests) may perhaps be explained as a cross-over point between these two factors, where the increase in concentration compared with 58% RH has increased the IR-drop within the droplet, but the chloride concentration is still not at its most aggressive to allow a critical corrosion chemistry to fully stabilize within a corrosion site.

Chloride dilution.—Although the inhibition mechanism of either nitrate or sulfate salts on pitting corrosion is not the focus of this work, it is worth highlighting an additional factor which may play a role under atmospheric conditions not found in full immersion tests. The concentration of a pure $MgCl_2$ droplet in equilibrium with an RH of 60% is ~7 M [Cl^-]. However, the chloride concentration in a mixed $MgCl_2$, $Mg(NO_3)_2$ droplet (Cl^-:NO_3^- = 1:1) in equilibrium with the same humidity is ~3.5 M (Figure 17a). Chloride concentration is known to be a key factor in pitting corrosion.[20,35] The 'dilution effect' of adding another salt into solution with a chloride salt, even if the added salt is not itself an inhibitor may change the chloride concentration of the solution for a given equilibrium RH such that corrosion does not take place. The effects of the inhibitors below cannot be fully explained by this phenomenon alone, but it is highlighted here as an additional factor to keep in mind when interpreting mixed salt systems under atmospheric conditions.

Droplet size.—Tests using both 4 μL and 2 μL droplets on 316L stainless steel were used in this study, with diameters of ~3.3 mm and ~2.3 mm, respectively. Larger droplets were more likely to cause corrosion; small droplets failed to cause corrosion at a humidity of 58%RH, while 48% of equivalent larger droplets caused corrosion under the same conditions. While this was not the main focus of the experiment, it may support the idea that corrosion is cathodically limited since increasing the droplet size increases the coverage of the electrolyte over the metal surface, thus increasing the available area for a cathodic reaction to take place.[21,29,36] As such, the propagation of initiation sites to stable and visible pits may be limited or even impeded under small droplets. Another factor may be that smaller areas of electrolyte are less likely to cover a suitable initiation site from which stable pitting can propagate.

It is also worth considering that the deposition method for the 2 μL droplets was different to that for the rest of the 4 μL droplets, in that the droplet area was pre-deposited with a $CaSO_4$ solution prior to the deposition of the chloride solution, which was then allowed to dry. It has been shown that the composition of the passive layer on 304 and 316 stainless steels can be affected by the exposure environment, specifically by the presence of a water layer. Cr enrichment has been found in the passive layer during the first stages of exposure to a wet-dry cycling process, which the deposition and then drying of a $CaSO_4$ solution may mimic.[37] As such, the passive layer present for the 2 μL droplets may well be of a composition more resistant to corrosion than that present for the 4 μL tests, where there was no pre-deposition of an aqueous solution before the deposition of chloride.

Alloy comparison.—Critical inhibition ratios for nitrate were found to be the same on both 304L and 316L alloys, within the experimental resolution (0.3, 1, 3 NDD:CDD ratios), though the fact that in control experiments 316L showed fewer instances of corrosion than 304L made it more difficult to evaluate any inhibition effects on this alloy.

In the case of sulfate, no inhibition was observed at 36% RH or 46% RH, but some evidence of inhibition was seen at 58% RH on both 304L (linear tests and logarithmic tests at CDD ≥250 μg/cm^2) and 316L (logarithmic tests). The ratio for inhibition from $MgSO_4$ on 316L was lower than that seen on 304L (0.1–0.3 compared with 0.3–0.5, SDD:CDD, respectively) and was independent of CDD. Corrosion under $MgSO_4$ precipitates was observed on 304L at 58% RH, and not observed (for the most part) in the same experiments on 316L. The total number of corroded droplets was less on 316L than on 304L. These differences in corrosion behavior are likely to be attributed to the addition of molybdenum in 316L, which acts to decrease susceptibility to pitting.[38,39]

Nitrate inhibition.—The inhibiting effects of nitrate on corrosion under chloride containing droplets are clear from both logarithmic and linear variation tests on 304L and 316L (Figure 9). The effective NDD:CDD inhibition ratio was seen to be dependent on the exposure humidity, with increasing humidity lowering the required ratio. While tests on 304L carried out in these studies can be considered easier to interpret than those obtained on 316L (due to the lower baseline incidence of pitting in the latter in control experiments in the absence of nitrate), similar values of the inhibition threshold were found on 304L and 316L.

The results based both on logarithmic tests at CDDs between 0.85 and 850 μg/cm^2, and on linear tests at a CDD of 1230 μg/cm^2, are summarized in Table V, which presents anion deposition density ratios required to obtained corrosion inhibition of all samples in a given condition (inhibition of corrosion in some but not all droplets was observed at lower values). Ratios are presented in terms of deposition density (a commonly measured parameter in atmospheric corrosion studies), deposited molar ratio, and calculated activity ratio.[18] The values from the linear and logarithmic variation tests are consistent, with the inhibition ratios found in the linear tests falling generally within the range observed by the logarithmic tests. The NDD:CDD inhibition ratio determined from the logarithmic tests is more reliable since there were 20 droplets for each condition rather than 4 for the linear tests. However, the finer composition increments of the linear tests suggest that the inhibition ratio is likely to be closer to the lower limit than the upper limit set by the logarithmic tests.

Examples of inhibition ratios for nitrate on 304 reported in other studies based on experiments in bulk solution are presented in Table VI. On a concentration (molar) basis, typical inhibition ratios (nitrate:chloride) are of the order of 0.2–0.4, which are somewhat lower than those observed at relative humidities of 35% and 46% in this study. At a higher humidity of 58% RH, however, the inhibition ratio approaches the upper end of those found in the literature. It is noteworthy that increasing the humidity (and hence the dilution of the droplet system) leads to conditions more similar to those typically present in tests in bulk solution, and results in lower values of the inhibition ratios, leading to values more similar to those found in the literature.

On an activity basis, results in bulk solutions found in the literature are more similar to those estimated in atmospheric conditions in this study across the RH range tested. In dilute conditions (high RH), again the predicted convergence with data from bulk solutions is somewhat unsurprising. The reasonable agreement in more concentrated solutions (lower RH), however, is an important result, and provides confidence in the inhibition ratios found in this study.

Few studies describe variation in critical inhibition ratio in different conditions, in particular in respect to solution concentration. An exception is the work of Leckie and Uhlig and Uhlig and Gilman, who

Table V. Summary of nitrate:chloride inhibition ratios for both logarithmic (304L and 316L together) and linear (304L) variation tests (Figure 9) on a mass, mole, and activity basis. Logarithmic tests summarize results obtained with CDDs between 0.85–850 μg/cm², showing the most conservative results (highest ratios), and give the range in which the inhibition ratio lies. Linear tests, at a CDD of 1230 μg/cm², give the inhibition ratio as the lowest nitrate:chloride ratio at which pitting was no longer observed. In all cases the inhibition ratios presented were those required to achieve inhibition for all samples tested, though some inhibition effects were observed at lower ratios. NO_3^-:Cl^- ratios are calculated from deposited solution composition. Activity ratios are calculated using OLI Analyser 9.2.[18]

	NDD:CDD			NO_3^-:Cl^-			$\{NO_3^-\}$:$\{Cl^-\}$		
Relative humidity	35%	46%	58%	35%	46%	58%	35%	46%	58%
Logarithmic variation (304L and 316L)	1–3	1–3	0.3–1	0.6–1.7	0.6–1.7	0.2- 0.6	>0.28*	0.33–1.1	0.12–0.39
Linear variation (304L)	1.6	0.9	0.7	0.9	0.5	0.4	0.47	0.29	0.26

*Activity ratio for the upper limit could not be calculated as solution is thermodynamically unstable.

developed a relationship between the inhibition ratio and the chloride activity.[7,11] However, they predicted that the critical $\{NO_3^-\}$:$\{Cl^-\}$ inhibition ratio would decrease as $\{Cl^-\}$ increases.[11] The opposite trend is seen in the present work, where a lower humidity, and thus a higher $\{Cl^-\}$, required a higher $\{NO_3^-\}$:$\{Cl^-\}$ ratio for inhibition. It is important to point out that this relation was calculated by Uhlig et al. via full immersion electrochemistry for anion activities below 1 (i.e. dilute conditions compared to atmospheric systems), and this may explain the discrepancy between it and the data derived from high concentration atmospheric testing produced in this work. It is worth noting that even the work undertaken at a chloride concentration of 3.12 M by Uhlig and Gilman is still not sufficient a concentration to cause pitting corrosion of 304L under atmospheric conditions using magnesium chloride.[20,29]

For droplets below the inhibition threshold, the amount of rust observed appeared to be independent of the amount of nitrate within the droplet (e.g. Figure 5). The extent of rust coverage is a reasonable proxy for pit volume, which was not measured in the current work. This suggests that nitrate addition does not have a significant effect on pit growth propagation kinetics but instead affects whether or not pits are stable at all. The addition of sufficient nitrate to an active pit solution has been shown to stifle pit growth and promote passivation in systems which have formed a salt layer, though active dissolution (i.e. no salt layer present) was not affected.[10,16] Nitrate has also been shown to eliminate slow rise electrochemical transients, associated with metastable pitting events which may form a salt layer.[9,40] Furthermore, nitrate has been shown to affect re-passivation kinetics on freshly scratched surfaces, with higher nitrate content leading to faster re-passivation.[40] In the current work, there was no gradual change in the amount of rust (and, by implication, pit volume) with increasing nitrate levels up to the point where complete inhibition occurred. This suggests that nitrate inhibits the early stage of pitting, possibly the metastable state, rather than pit propagation. This hypothesis is consistent with the idea that metastable pits contain a salt layer, and the observation that nitrate inhibits pitting in the presence of a salt layer rather than in the active state.[10,41]

Sulfate inhibition.—The inhibition effects produced by sulfate were more variable than those produced by nitrate. The data for 316L at 58% RH represent the only case where the exposure humidity affected the SDD:CDD critical inhibition ratio in a manner similar to that for nitrate. Moreover, inhibition was only observed with $MgSO_4$, not with $CaSO_4$. In environments containing calcium (such as concrete buildings), sulfate is expected to be present in the form of $CaSO_4$, originating from concrete dust.[3] Tests carried out on with both $CaCl_2$ and $MgCl_2$ mixed with $CaSO_4$ solutions indicated that, due to its low solubility, the presence of $CaSO_4$ is unlikely to lead to inhibition under a wide range of atmospheric conditions.

Table VII summarizes data for the effects of magnesium sulfate on the inhibition of corrosion for both logarithmic variation tests (CDDs between 0.85–850 μg/cm²) and linear variation tests (CDD fixed at 1230 μg/cm²). Magnesium sulfate was not clearly seen to act as a corrosion inhibitor at humidity of either 36% RH or 46% RH on either 304L or 316L. At 58% RH inhibition was observed on both alloys.

On 304L, the critical SDD:CDD ratio (on a deposition density basis) was between ~0.3–1 and was only observed at high CDD (250–1230 μg/cm²). The reason for the effect of CDD on the inhibiting effects of sulfate on 304L is unclear, though it is important to note that these levels of CDD are higher than those expected to develop in storage facilities for the majority of their service.[3] At high SDD:CCD ratios (>2). precipitation of magnesium sulfate removed any inhibiting effects (Figure 13e and Figure 15).

On 316L, comparison of control tests with tests containing sulfate indicated that, like in 304L, some inhibition was obtained at the highest RH tested (58%). At this RH, the SDD:CDD inhibition ratio was between ~0.1–0.3, which is slightly lower than that estimated for 304L. In this case, however, inhibition was also observed at lower CDD values and almost no corrosion was seen to occur under droplets containing magnesium sulfate precipitates at high SDD:CDD ratios (1 corrosion site in 40 droplets, Figure 13f), indicating that precipitation had little effect on the inhibition provided (notwithstanding the limited inherent reliability of tests on 316L).

Examples of inhibition ratios for sulfate on 304 reported in other studies in bulk solution are presented in Table VIII. On a concentration (molar) basis, typical inhibition ratios are of the order of 0.2–10 for sulfate, which are very scattered and substantially higher than those found in this study. One reason for this may be the definitions used for 'inhibition' in some of the electrochemical tests in the literature, being a condition under which no pitting was observed up to the largest applied potential (e.g. ~800 mV vs. Ag-AgCl).[13] In compar-

Table VI. Summary of literature data on pitting inhibition ratios on 304 stainless steel and similar alloys for nitrate – chloride solutions.[43]

Alloy	Temperature (°C)	NO_3^-:Cl^-	$\{NO_3^-\}$:$\{Cl^-\}$	Maximum $[Cl^-]$(mol/L)	Reference
18Cr-8Ni	25	0.4	–	0.56	Rosenfeld and Danilov 1967[12]
304	25	–	0.24	1.0	Leckie and Uhlig 1966[11]
304	25	0.2	–	0.5	Yashiro et al. 1997[13]
304*	25	0.2	–	0.2	Bobić and Jedić 2005[14]
18Cr–8Ni	–	–	0.2	3.12	Uhlig and Gilman 1964[7]

*= an alloy similar to Type 304.

Table VII. Summary of sulfate:chloride inhibition ratios for both logarithmic (CDDs between 0.85–850 μg/cm^2, 316L and 304L separately) and linear (CDD of 1230 μg/cm^2, 304L) variation tests (Figure 13 and Figure 15). Both tests give the range in which the inhibition ratio lies. Values where an inhibition range was only observed at high CDD conditions (250 – 850 μg/cm^2 on logarithmic tests, 1230 μg/cm^2 on linear tests) are marked with an asterisk (*). SO_4^{2-}:Cl^- ratios are calculated from deposited solution composition. Activity ratios could not be calculated as several solution compositions were thermodynamically over-saturated.

	SDD:CDD			SO_4^{2-}:Cl^-		
Relative humidity	35%	46%	58%	35%	46%	58%
Logarithmic variation (316L)	X	X	0.1–0.3	X	X	0.04–0.11
Logarithmic variation (304L)	X	X	0.3–1*	X	X	0.11–0.37*
Linear variation (304L)	X	X	0–0.5*	X	X	0-0.18*

X = No inhibition observed.
*= Inhibition only observed at high CDDs (>250 μg/cm^2).

ison, in this work all that may be required to inhibit corrosion is the raising of the pitting potential above that able to be supplied by the droplet. As such the upper values given in Table VIII may be overestimates for a droplet system. Furthermore the pH of the electrolyte solutions may have an effect on the critical inhibitor ratio, as suggested by Rosenfeld and Danilov (though it is interesting to note that Leckie and Uhlig disagree that there is any effect from neutral to low pH).[11,12] Not all studies report the pH of their testing solutions, which may introduce some uncertainty in interpreting the current literature data.

According to studies in bulk electrolytes,[11] the critical activity ratio for inhibition of sulfate to chloride increases with increasing chloride activity (the opposite to what was predicted in nitrate systems, but the same relation as has been found for nitrate systems in the current work), suggesting that the higher chloride concentrations obtained at low humidities would require higher SDD:CDD ratios.[34] This was observed in the current work, where sulfate:chloride ratios which had inhibited corrosion at 58% RH did not inhibit at 47% RH. Given the limited solubility of sulfate salts, there is therefore a more limited range of humidities where inhibition can be expected to occur, as a solution in equilibrium with a low humidity cannot hold sufficient sulfate in the aqueous phase as would be required to inhibit corrosion. If the values listed in Table VIII are indeed representative of a sulfate:chloride inhibition ratio, then it is likely that such solution ratios are only achievable under conditions of high humidity, where both chloride and sulfate species can remain in solution without precipitating.[34]

There were indications that corrosion product coverage was reduced in droplets with sulfate contents close to the inhibition/precipitation ratio. This was most clearly seen on the linear tests. This suggests that sulfate may affect the propagation of active pits.[42] However, the limited statistics of these tests suggests further work should be done in order to deliver robust ratios.

Solution precipitation.—Additional complexity in the interpretation of these tests is associated with the case of corrosion following precipitation of salts. In static humidity tests (such as those presented here) in which precipitation was observed to develop over time, precipitation occurs as a result of solution supersaturation. In mixed salt solutions, precipitation depends on both the humidity and the ratio of salts (it does not depend on the total deposition density of different salts). These factors will affect whether, when precipitation starts, salts containing inhibitor or chloride will form, followed, at the efflorescence point, by precipitation of both inhibitor-containing and chloride-containing salts (see below). For a given IDD:CDD ratio (where IDD is "inhibitor deposition density", representing either nitrate or sulfate), the effect of precipitation in removing ions from solution should be independent of the deposition density of each salt.

For $MgCl_2 + Mg(NO_3)_2$ mixtures, in droplets at NDD:CDD ratios $\gtrsim$3, precipitation was observed at 36% RH and 46% RH, though two instances of precipitation at NDD:CDD ratios <3 were observed (Figure 6b). At 36% RH on 304L corrosion was observed under some of these droplets. This indicates that, even when saturated in inhibitor, a solution containing a solid salt phase can undergo corrosion. In the case of nitrate salts, corrosion under precipitates was only observed at low humidities (36% RH) and may affect the corrosion behavior of stainless steel in relatively dry conditions.

Much more substantial precipitation was observed in sulfate solutions. In the case of $MgSO_4$ on 304L, inhibition was only observed at relatively high humidities (58% RH) and CDDs (>250 μg/cm^2) but was effectively lost at higher SDD:CDD ratios when precipitation occurred. In a droplet containing both aqueous and solid sulfate phases, the aqueous phase must be at saturation. It is notable that inhibiting effects were lost when saturation was observed, even though the solution concentration of sulfate was theoretically at its maximum value, and had shown inhibiting effects previously. This suggests that either (a) a greater inhibition ratio is required to prevent corrosion underneath solid deposits or (b) the systems which showed evidence of sulfate inhibition were in fact super-saturated, and the precipitation brought the aqueous solution sulfate content down below inhibiting levels.

Thermodynamic modelling of these binary salt systems does indicate that super-saturation of droplets was occurring in systems just beyond thermodynamic saturation. Figure 6a shows experimental data overlaid with the theoretical saturation point of $Mg(NO_3)_2$ under these conditions. While precipitation was observed in some cases in systems above this threshold, it was not seen in all cases, suggesting

Table VIII. Summary of literature data on pitting inhibition ratios on 304 stainless steel and similar alloys for sulfate – chloride solutions.[43]

Alloy	Temperature (°C)	SO_4^{2-}:Cl^-	{SO_4^{2-}}:{Cl^-}	Maximum [C^-](mol/L)	Reference
18Cr-8Ni	25	2,10*	–	0.56	Rosenfeld and Danilov 1967[12]
304	25	–	1.15	1.0	Leckie and Uhlig 1966[11]
304	25	0.2–5	–	0.5	Yashiro et al. 1997[13]
304**	25	5	–	0.2	Bobić and Jedić 2005[14]

*Inhibition ratios varied with pH, with ratios of 2 observed for pHs of 2 and 12, and a ratio for 10 observed for a pH of 7.
**an alloy similar to type 304.

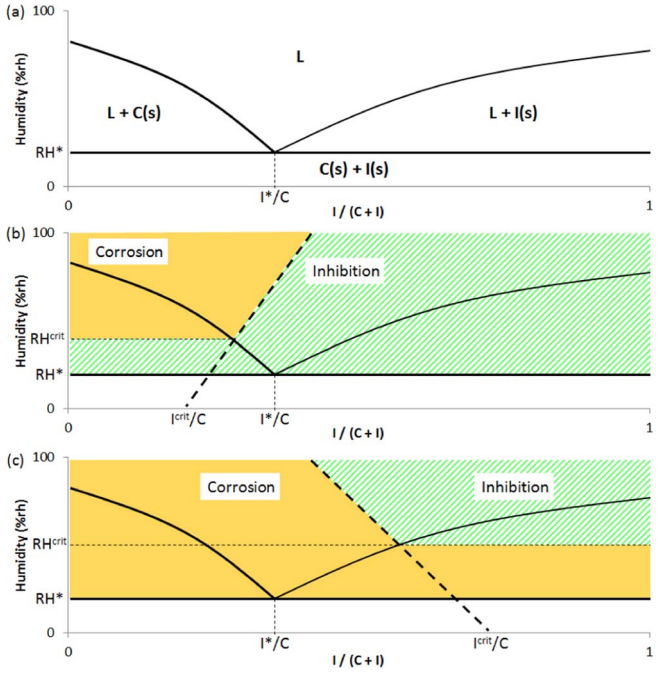

Figure 18. Schematics of the (a) phase and (b,c) possible corrosion behaviors of a general mixed salt system, composed of salts I (inhibitor) and C (chloride), in relation to the equilibrium ambient humidity. I^*/C is the eutectic point of the system; the I^{crit}/C line (b,c) is defined as the solution ratio over which corrosion is inhibited, for which two specific dependences on RH are assumed for illustrative purposes.

that some droplets were maintaining a thermodynamically unstable concentration of salts.

Mixed salt phases at variable humidities.—In single salt systems, the humidity and deposition density together control the extent/continuity of any moisture film or droplet developed on exposed surfaces, which controls the overall amount of cathodic surface able to drive corrosion damage and hence the extent of damage (as noted in other studies as well as in this study).[2,21,36] In studies with mixed salts, however, the relative deposition density of different salts also affects the wetting behavior of the system.

Figure 18a shows a schematic phase diagram of a binary system containing salts I (inhibiting salt) and C (chloride salt), which have no mutual solubility in the solid phase, as a function of composition. The eutectic point is at RH^* and a concentration fraction I^*/C. This is the lowest RH at which a liquid phase can be found. To the left of this composition (an overall composition rich in C), in the L+C(s) region, solid C will be found, with a solution concentration (given by the tie line to the liquidus) that is richer in I than the overall composition. To the right of the eutectic composition (overall composition richer in I), in the L+I(s) region, solid I will be found with a solution composition given by the tie line that is richer in C than the overall composition. However, in the liquid region (L), the composition of the solution is identical to the overall composition.

The corrosion behavior of a mixed salt droplet can be considered by assuming that there is a critical ratio of inhibitor:chloride, I^{crit}/C, required to inhibit corrosion (this value may vary with RH). Two systems with different example inhibitors (and inhibitor behaviors) are shown in Figure 18. In general, it is the absolute I/C ratio on the surface and its relationship with I^{crit}/C which is of prime importance in predicting corrosion behavior. Depending on the variation of I^{crit}/C with RH, however, the humidity may still need to be taken into account, both in terms of changes in inhibition ratios as a function of concentration/activity (as seen in this work for nitrate) and, at relatively low RH, in terms of any precipitation effects that may occur.

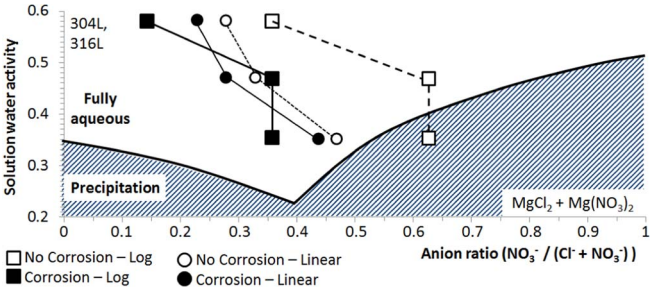

Figure 19. Saturation conditions for a $MgCl_2 + Mg(NO_3)_2$ mixed salt system. Calculated at 30°C using OLI Analyser 9.2, MSE database. Corrosion and inhibition data on both 304L and 316L alloys has been overlaid (data from Figure 9). Solution water activity is equivalent to equilibrium relative humidity, i.e. water activity x 100 = RH%.

Figure 18b shows a system where I^{crit}/C crosses the liquidus line to the left of the eutectic (I^*/C). In such a system, variations in humidity will never cause sufficient inhibitor salt to be precipitated, and thus removed, from the liquid phase to allow corrosion (i.e. to bring I/C below I^{crit}/C). In this case, the dependence of the corrosion behavior on the RH may be limited, though the variation of I^{crit}/C with RH in this example does allow the system to become uninhibited for certain values of I/C at higher RHs. Figure 18c, conversely, shows an inhibitor with I^{crit}/C crossing the liquidus to the right of the eutectic point. In this system, even in inhibitor-rich systems (i.e. $I/C > I^{crit}/C$), sufficiently low RH may cause I (the inhibitor salt) to precipitate, removing it from solution and potentially allowing the solution composition to decrease below I^{crit}/C. In such a case, both the salt ratios and the humidity are of key importance in predicting the corrosion behavior of the system.

These considerations illustrate a simple I^{crit}/C dependence on RH, and it should be highlighted that any real dependence may be more complex than a simple linear relation. It also assumes that the formation of precipitates has no effect on the value of I^{crit}/C. If this is not the case, the system will display additional complexity, displaying a larger number of possible behaviors but also becoming more difficult to generalize (i.e. the complexity will depend on the functional form of the solution concentration (I/C), and inhibition ratio (I^{crit}/C), with the relative humidity).

Figure 19 and Figure 20 show thermodynamic saturation curves for $MgCl_2 + Mg(NO_3)_2$, and $MgCl_2 + MgSO_4$ systems, respectively, together with the experimental data obtained in this work. For the nitrate system, the data points show experimental findings for corrosion and inhibition as a function of water activity (determined from RH) and anion fraction taken from Figure 9 (largely based on 304L, but considered applicable to 316L). For the sulfate system, results from the linear tests on 304L and the logarithmic tests on 316L have been shown.

The nitrate system in Figure 19 shows similarities with the model system suggested in Figure 18c, with I^{crit}/C increasing with decreasing RH, and crossing the liquidus to the right of the eutectic point. In the

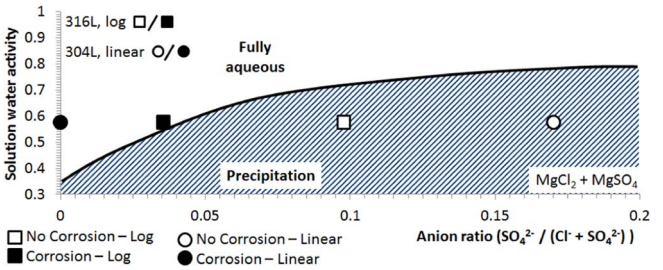

Figure 20. Saturation conditions for a $MgCl_2 + MgSO_4$ mixed salt system. Calculated at 30°C using OLI Analyser 9.2, MSE database. Corrosion and inhibition data for 316L (logarithmic tests, squares) and 304L (linear tests, circles) have been overlaid. Solution water activity is equivalent to equilibrium relative humidity, i.e. water activity x 100 = RH%.

conditions tested, any dependence of the inhibition effect from the relative humidity is likely to be associated with changes in anion activity as a function of RH rather than precipitation effects, although precipitation effects may be expected to potentially play a role at particularly low RH.

The sulfate system in Figure 20, conversely, lacks sufficient data to establish an I^{crit}/C trend, although it is interesting to see that inhibition was observed in conditions where sulfate precipitation was expected (based on thermodynamic calculations) but not observed. As such, one may conclude that inhibition was only seen in cases of supersaturation, and not in thermodynamically stable conditions.

It is clear that, in order to fully assess atmospheric systems consisting of mixed salts, thermodynamic modelling is a key tool to predict and interpret the appearance of different chemical phases from solution, and to give insight as to the evolution of corrosion behavior when the exposure conditions of these systems changes. In this work, thermodynamic calculations (in line with the well-established theory of phase separation) and experimental work have shown that a liquid phase containing a corrosion inhibitor (either nitrate or sulfate in this work) may be present in mixed salts below the saturation point (i.e. at lower RH) of the inhibiting salt, thus affording some corrosion protection. Precipitation/dissolution of either corrosive and/or inhibiting salts as the RH varies will change the chemistry of the aqueous solution, with the potential to increase or decrease the amount of inhibitor present in solution, and so affect whether or not corrosion will occur.

Combinatorial droplet tests have been shown in this study to be an excellent method for investigating such atmospheric systems, allowing a large range of variables (absolute deposition densities, inhibitor:chloride ratios, alloy, inhibitor type, exposure RH) to be combined with high levels of statistical robustness in order to deliver results with confidence.

Conclusions

Experiments were carried out on 304L and 316L stainless steels to assess the ability of nitrate and sulfate to act as corrosion inhibitors for atmospheric corrosion in chloride-containing environments. Tests were carried out at 31°C in a range of humidities (between 35–75% RH) with mixtures of chloride salts ($MgCl_2$ and $CaCl_2$) and inhibiting salts ($MgNO_3$, $MgSO_4$ and $CaSO_4$) as well as in the absence of inhibiting salt (control experiments). Deposition densities of chloride tested ranged between ~8 and 1,200 $\mu g/cm^2$, compared with levels up to 100 $\mu g/cm^2$ expected to be relevant to the specific problem studied (the storage of ILW containers). The results of this study indicate that:

- Magnesium nitrate acts as a corrosion inhibitor on both 304L and 316L at all humidities tested (between 35% to 58% RH), when the ratio between the nitrate deposition density and the chloride deposition density (NDD:CDD, anion mass per unit area) is above a critical value. This critical value generally decreases as the relative humidity increases, and is similar for both 304L and 316L. The critical inhibition ratio on a mass basis was in the range ~1–3 at 36% RH and 46% RH, and ~0.3–1 for 58% RH, judged across a range of CDDs (0.85–850 $\mu g/cm^2$).
- Magnesium sulfate does not act as a corrosion inhibitor for either 304L or 316L at humidities of 36% RH or 46% RH. At 58% RH sulfate inhibited corrosion of 316L at a critical sulfate:chloride deposition density ratio (SDD:CDD, anion mass per unit area) within the range ~0.1–0.3. Sulfate also inhibited pitting of 304L at 58% RH at a critical SDD:CDD ratio between ~0.3 and 0.5, though only when the CDD was high, between 250 and 1230 $\mu g/cm^2$. In general, the behavior of magnesium sulfate in these tests was not straightforward to ascertain, given its tendency to precipitate and indications that, when achieved, inhibition was associated with supersaturated solutions (see below).
- Precipitation of nitrate and particularly sulfate salts occurred in high IDD:CDD systems, depending on humidity, and under some droplets caused a loss of corrosion inhibition. This is suggested to be caused by either the formation of a more stable corrosion environment under precipitates (i.e. crevice or under-deposit corrosion), or as evidence of previous super-saturation of inhibitor in solution.
- A model for the interaction and development of chloride/inhibitor systems under varying humidities was developed based on thermodynamic calculations, for use in predicting the behavior of such systems under conditions close to and beyond saturation.
- Preliminary work on the role of calcium sulfate deposits on atmospheric corrosion did not give any indication that their presence influenced pitting susceptibility of 316L stainless steel in the presence of either magnesium or calcium chloride, but further work is required to confirm this.

Acknowledgments

The authors thank Fraser King (Integrity consulting Ltd.), Kevin Christie and Cliff Harris (Amec Foster Wheeler) and Trevor Rayment (Diamond Light Source Ltd.) for useful discussions. The work was funded by EPSRC (grant EP/I036397/1) and Radioactive Waste Management Ltd. (Contract NPO004411A-EPS02). Supplementary data may be accessed via http://epapers.bham.ac.uk/2952/.

References

1. Nuclear Decomissioning Authority, *Geological Disposal: Package Evolution Status Report*, NDA/RWMD/031, 2010.
2. C. Padovani, O. E. Albores-Silva, and E. A. Charles, *Corrosion*, **71** (3), 292 (2015).
3. C. Padovani, R. J. Winsley, N. R. Smart, P. A. H. Fennell, C. Harris, and K. Christie, *Corrosion*, **71** (5), 646 (2015).
4. R. P. V. Cruz, A. Nishikata, and T. Tsuru, *Corrosion Science*, **38** (8), 1397 (1996).
5. R. P. V. Cruz, A. Nishikata, and T. Tsuru, *Corrosion Science*, **40** (1), 125 (1998).
6. T. Prosek, A. Le Gac, D. Thierry, S. Le Manchet, C. Lojewski, A. Fanica, E. Johansson, C. Canderyd, F. Dupoiron, T. Snauwaert, F. Maas, and B. Droesbeke, *Corrosion*, **70** (10), 1052 (2014).
7. H. H. Uhlig and J. R. Gilman, *Corrosion*, **20** (9), 289t (1964).
8. G. O. H. Whillock, T. J. Binks, and C. J. Donohoe, *Corrosion*, **68** (11), (2012).
9. R. S. Lillard, G. Vasquez, and D. F. Bahr, *Corrosion*, **66** (7), (2010).
10. S. R. Street, W. C. Xu, M. Amri, L. Y. Guo, S. J. M. Glanvill, P. D. Quinn, J. F. W. Mosselmans, J. Vila-Comamala, C. Rau, T. Rayment, and A. J. Davenport, *Journal of the Electrochemical Society*, **162** (9), C457 (2015).
11. H. P. Leckie and H. H. Uhlig, *Journal of the Electrochemical Society*, **113** (12), 1262 (1966).
12. I. L. Rosenfeld and I. S. Danilov, *Corrosion Science*, **7** (3), 129 (1967).
13. H. Yashiro, A. Oyama, and K. Tanno, *Corrosion*, **53** (4), 290 (1997).
14. B. Bobić and B. Jegdić, *Scientific-Technical Review*, **55** (3), 3 (2005).
15. C. S. Brossia and R. G. Kelly, *Corrosion*, **54** (2), 145 (1998).
16. R. C. Newman and M. A. A. Ajjawi, *Corrosion Science*, **26** (12), 1057 (1986).
17. R. C. Newman and T. Shahrabi, *Corrosion Science*, **27** (8), 827 (1987).
18. OLI Systems, 2015.
19. T. V. Nam, E. Tada, and A. Nishikata, *Journal of the Electrochemical Society*, **162** (9), C419 (2015).
20. Y. Tsutsumi, A. Nishikata, and T. Tsuru, *Corrosion Science*, **49** (3), 1394 (2007).
21. N. Mi, M. Ghahari, T. Rayment, and A. J. Davenport, *Corrosion Science*, **53** (10), 3114 (2011).
22. S. Hastuty, Y. Tsutsumi, A. Nishikata, and T. Tsuru, *ISIJ Int.*, **52** (5), 863 (2012).
23. X. X. Fu, J. H. Dong, E. H. Han, and W. Ke, *Sensors*, **9** (12), 10400 (2009).
24. G. S. Frankel, M. Stratmann, M. Rohwerder, A. Michalik, B. Maier, J. Dora, and M. Wicinski, *Corrosion Science*, **49** (4), 2021 (2007).
25. E. Schindelholz and R. G. Kelly, *Electrochemical and Solid State Letters*, **13** (10), C29 (2010).
26. B. E. Risteen, E. Schindelholz, and R. G. Kelly, *Journal of the Electrochemical Society*, **161** (14), C580 (2014).
27. S. Shoji and N. Ohnaka, *Corrosion Engineering*, **38** (2), 92-7 (1989).
28. M. Gunther, N. P. C. Stevens, G. McFiggans, and A. B. Cook, *Corrosion Engineering Science and Technology*, **49** (6), 509 (2014).
29. B. Maier and G. S. Frankel, *Journal of the Electrochemical Society*, **157** (10), C302 (2010).
30. F. King, P. Robinson, C. Watson, J. Burrow, and C. Padovani, *NACE International*, **Corrosion/2013** (paper no. 2717), (2013).
31. AMEC, *Investigation Into the Atmospheric Corrosion of Stainless Steel ILW containers – Tests With Salt Mixtures and in Conditions of Cyclic Relative Humidity*, 17391/TR/0009-4, 2016.
32. ASTM, *E104-02(2007) "Standard Practice for Maintaining Constant Relative Humidity by Means of Aqueous Solutions"*, 2007.
33. S. R. Street, N. Mi, A. J. M. C. Cook, H. B. Mohammed-Ali, L. Guo, T. Rayment, and A. J. Davenport, *Faraday Discuss.*, **180** (0), 251 (2015).
34. P. Pohjanne, L. Carpén, T. Hakkarainen, and P. Kinnunen, *Journal of Constructional Steel Research*, **64** (11), 1325 (2008).
35. Y. Tsutsumi, A. Nishikata, and T. Tsuru, *Journal of The Electrochemical Society*, **152** (9), B358 (2005).
36. Z. Y. Chen and R. G. Kelly, *Journal of The Electrochemical Society*, **157** (2), C69 (2010).
37. R. H. Jung, H. Tsuchiya, and S. Fujimoto, *ISIJ Int.*, **52** (7), 1356 (2012).

38. C. Clayton and O. lngemar, in *Corrosion Mechanisms in Theory and Practice*, Third Edition, p. 327, CRC Press, (2011).
39. R. C. Newman, *Corrosion Science*, **25** (5), 331 (1985).
40. R. S. Lillard, G. Vasquez, and D. F. Bahr, *Journal of the Electrochemical Society*, **158** (6), C194 (2011).
41. P. C. Pistorius and G. T. Burstein, *Philos. Trans. R. Soc. Lond. Ser. A-Math. Phys. Eng. Sci.*, **341** (1662), 531 (1992).
42. P. C. Pistorius and G. T. Burstein, *Corrosion Science*, **33** (12), 1885 (1992).
43. F. King, e-mail to A. Cook, (26/02/2014).